Rodrigo Badínez
Master in Photonics Programme
LTH, Lund University

PHOTOMETRIC EVALUATION AND CALIBRATION OF THE EARTHSHINE TELESCOPE

MASTER THESIS

Supervisors: Ahmad Darudi and **Torben Andersen**
Department of Astronomy and Theoretical Physics,
Lund Observatory,
Lund University.

Abstract

An earthshine telescope has been designed and is being fabricated at Lund Observatory in collaboration with the Danish Meteorological Institute. The instrument will measure the albedo of the Earth by observing the Moon in white light and in certain spectral bands.
The measurement is based on relative photometry of the dark and bright sides of the Moon, so the optical design of the telescope has been carried out with special attention to photometric quality and stray light performance. In addition, advanced operating modes have been developed. Hence, the instrument is expected to be superior to existing earthshine telescopes.

The LO/DMI Earthshine Telescope was envisaged to provide produce albedo measurements with an accuracy on the order of 0.1%. The objective of this thesis was to evaluate the accuracy of some of the main elements that contributes to the final photometric performance of the Earthshine Telescope. In particular the performance of the shutter was analyzed, since it is very crucial to obtain accurate photometry of the observation, especially due to the high range of the exposures from 10ms to few minutes which is needed for the albedo calculation. Also the proper characterization of the spectral filters transmission is very important for the precision of the spectro-photometric analysis of the Earth's albedo, and for this reason spectral measurements were done for all the filters of the Earthshine Telescope.

It was found that for 10ms the accuracy of the shutter response is 0.4%, and this will affect the accuracy of some of the operating modes of the Earthshine Telescope that require short exposures times. Nevertheless it is possible to decrease the error in shutter response for these operating modes by reducing the amount of light falling into the detector using a neutral density filter or reducing the aperture.

Also spectral characterization of all the color filters and Knife Edge Optical Density filters of the Earthshine Telescope was done, obtaining spectral curves that matched very well with the specified by the manufacturers.

Table of Contents

1. Introduction

In the last years the debate about global warming has been intensified and the fact that anthropogenic climate change is occurring is now a scientific consensus [1]. Reinforced efforts are been directed now to monitor and predict its consequences, and to achieve this climate models are essential.

The Earth's climate is governed by the balance between the incoming and outgoing energy fluxes on the planet. The incoming power depends on the amount of solar radiation coming from the Sun as well as on the reflectivity of the Earth. The outgoing power is emitted into the space at long wavelengths and it depends on the Earth's average temperature and on the amount of greenhouse effect [2].

Hence there are three main variables for the global climate model: the amount of solar irradiation, the reflectivity of the planet (albedo), and the amount of greenhouse effect. In the simplest view these variables will determine the global climate. However these variables are not entirely independent and changes in the global climate will also alter the albedo and the amount of greenhouse effect on the planet, and these interdependent interactions are not well known [3].

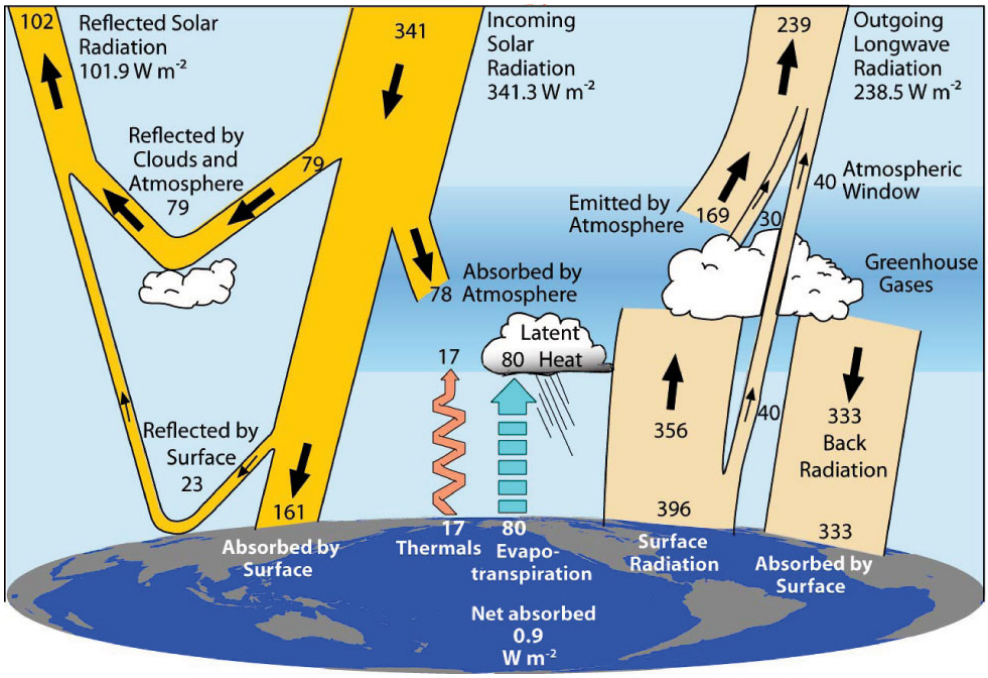

Figure 1 - The global annual mean energy balance of the Earth [4]. Radiation and heat fluxes in W/m^2.

Consequently, it is necessary to monitor these variables in order to produce accurate models that will predict correctly the upcoming global climatic changes. The LO/DMI[1] Earthshine Telescope project is aimed to contribute in this endeavour performing measurements of the terrestrial albedo.

[1] Lund Observatory and Danish Meteorological Institute respectively

The **albedo** of a planet is defined as the ratio of the energy reflected in any direction to the energy incident on its geometric cross section (Bond albedo [5]). If a 1% of change in the mean long term Earth's albedo is produced, it will result in an average temperature change of 0.5K on the Earth [6]. Moreover, data collected by satellites shows that the global mean Earth's albedo has an intrinsic daily variability about 1.6% due to the non-uniform distribution of the sources of the reflectivity through the globe (land, oceans, cloud cover, etc) and also it has a seasonal variability across the year [3]. For all these reasons, high accuracy albedo measurements are needed.

The objective of the Earthshine telescope is to monitor the Earth's albedo observing simultaneously (or within a short time interval) the moon area illuminated by the Sun together with the dark moon area tenuously illuminated by the Earth´s albedo. Due to the huge difference between the brightness of both areas it is indispensable that the detector has a very broad dynamic range along with good linearity in order to produce data with the necessary exactitude to achieve reliable values of the terrestrial albedo. The goal of the Earthshine Project is to obtain a precision of 0.1% in the albedo measurements.

In our project the calculation of the Earth´s albedo is based on the ratio of the measured earthshine irradiance on the dark side (DS) and sunlit irradiance on the bright side (BS) of the Moon image; this data can be acquired consecutively measuring one frame for each side of the Moon, or simultaneously using a single frame. Because of the short integration time needed to avoid saturation in the BS exposure, the use of a fast shutter is essential to properly control the exposure time and to avoid smearing effect. For this reason, the Uniblitz VS25 shutter with nominal opening and closing times of 3ms and 2ms respectively was chosen for this project. For this diploma project an examination of the shutter response was executed including calibration and stability analyses.

As the difference of intensities between the bright and dark side of the moon is so enormous, direct simultaneous observation using a CCD camera is not possible; the ratio between the BS and DS of the moon is typically higher than 10 000:1 [3] and this exceeds the dynamic range of even the better CCD cameras.

The LU/DMI Earthshine telescope has different operational modes that use different approaches to treat this problem. The more innovative one is the use of reflective neutral optical density filters to reduce the intensity on the BS of the moon [7]. These neutral density filters are called Knife Edge Density Filters (KEDF) because they are designed to cover only a part of the field of view of the telescope; for this reason they are placed at the first focal plane of the telescope.

The measurements of Earth's albedo can provide additional information if spectral information is obtained. For this reason, spectro-photometric capability is available in the Earthshine telescope by virtue of the set of 4 color filters, which can provide information about the nature of the reflective surfaces creating the albedo (determining the amount of reflection caused by the cloud cover, land, oceans, ice-snow, vegetation etc.).

Analysis of the transmittance of the filters was an important task of the current diploma work. Spectral analysis was performed for the color filter as well for the knife edge optical density filters.

1.1 Structure of the report

The current document is divided in four chapters plus one appendix:

- Chapter 1 is the introduction about the Earthshine telescope project and the diploma work.
- Technical information about the Earthshine telescope is given at Chapter 2. It also briefly explains how the albedo values can be calculated from the earthshine measurements.
- Chapter 3 is devoted to the analysis of the shutter response, in order to check its nominal characteristics and suitability for the Earthshine telescope.
- Chapter 4 is dedicated to the spectral transmission analysis of the color filters and knife edge optical density filters of the Earthshine telescope.
- Chapter 5 summarizes the conclusions of this diploma work.
- The Appendix contains additional information related to the experiments. In particular the specifications of the used spectrometer and the spectral curves of the filters from the manufacturers are included, together with the full-page versions of the measured spectral curves.

2. Lund Earthshine Telescope

The LU/DMI Earthshine telescope is a collaborative effort between Lund Observatory and The Danish Meteorological Institute. It has been designed to be a remotely controlled highly automated robotic telescope, which could be deployed to operate in almost any site of the world. The main goal of the project is to provide a tool to monitor the Earth's albedo by measuring the earthshine in the Moon. The design was initiated in 2006 and the first prototype will go into operation during the year 2011. Currently this first prototype is being tested at the optical laboratory of Lund Observatory, and if its performance is satisfactory then replicas of the telescope will be constructed and deployed around the word to provide global coverage of the albedo measurements [6].

2.1 General Characteristics

The Earthshine telescope is a relative small refractor with a lens system of three elements that produces two different image planes. In the first image plane a wheel is located with a hard knife edge and knife edge neutral density filters; in the second one the CCD camera is situated. Its optical layout is shown in Figure 2.

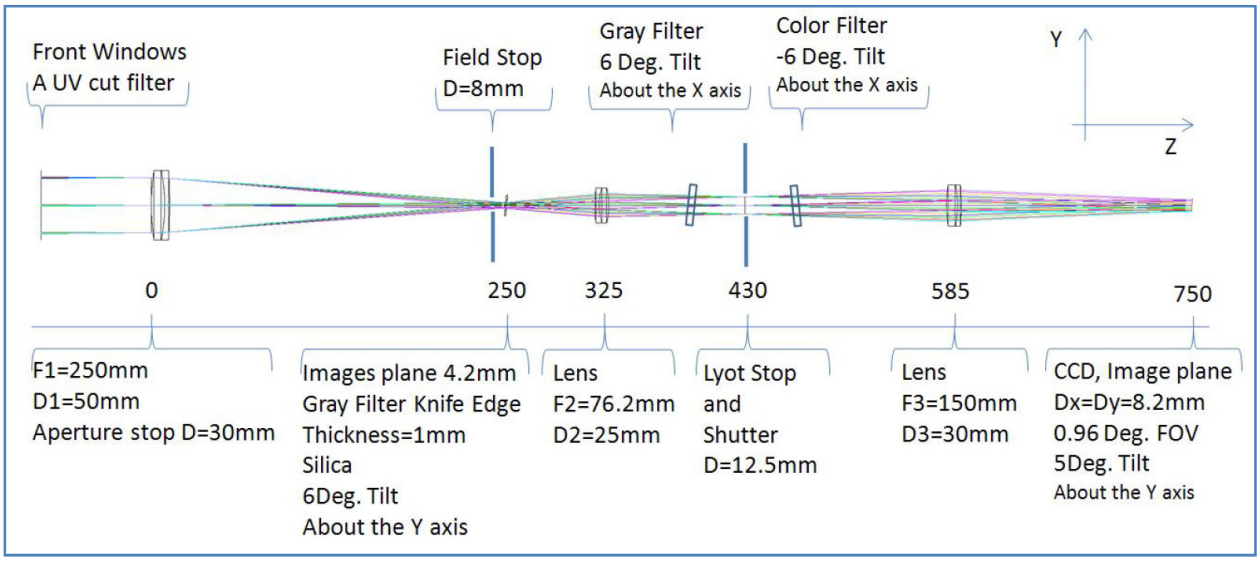

Figure 2 – Optical layout of the Earthshine Telescope [7]

The main components of the current LU/DMI Earthshine telescope are:

- CCD camera model Andor iXon 897-BV
- Astro-Physics 1200GTO German equatorial mount
- Lens system:
    - Objective: Thorlabs achromatic lens of 50mm diameter and 250mm focal length, with VIS-NIR AR coating
    - First relay lens: Thorlabs achromatic lens of 22mm diameter and 76.2mm focal length with VIS-NIR AR coating

    - Second relay lens: Edmund optics 30mm diameter and 150mm focal length achromatic lens with VIS-NIR AR coating
- Uniblitz VS25 electro-mechanical shutter
- 3 Knife edge optical density filters specifically manufactured for the project by *Ferroperm Optics A/S* with optical nominal densities of 3.5, 3.75 and 4, and one Hard Knife edge filter.

- Color filters from *Asahi Spectra Co.*:
    - JOHN-V-25
    - JOHN-B-25
    - Shortpass filter 750nm
    - Longpass filter 750nm
- Grey optical density filter (not yet installed)

There are two filter wheels with 6 positions each one to provide selectivity for the filters, located at the positions indicated in Figure 2 and Figure 3. A Lyot stop is implemented using an adjustable iris diaphragm for reduction of diffraction of entrance aperture (which is located in front of the objective, see Figure 3) and stray light in the system.

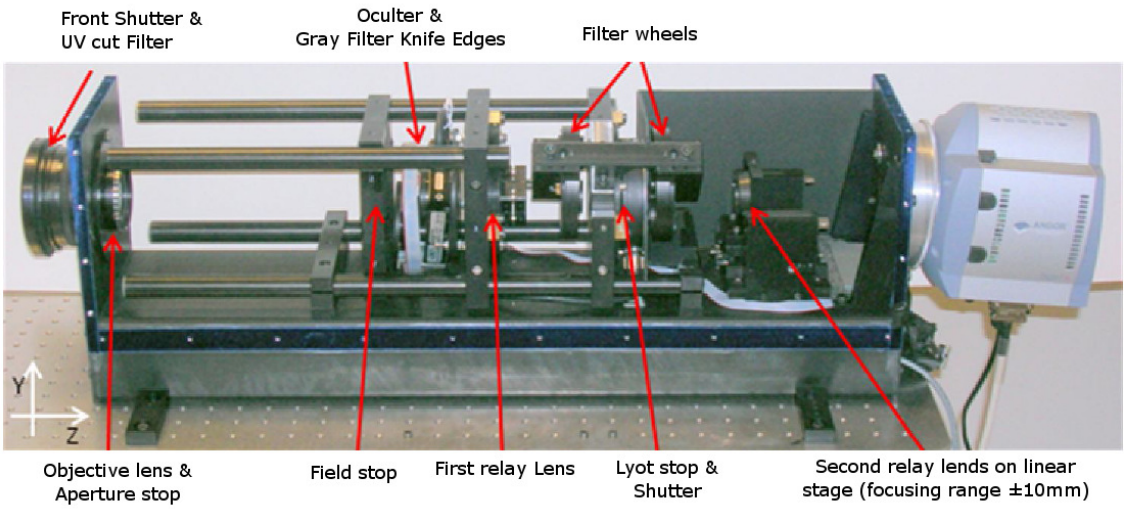

Figure 3 - Photo of the LU/DMI Earthshine telescope withput cover [7]

An electromechanical system composed by two rotary stages is in charge of the selection and orientation of the KEDFs; its schematic diagram is shown in Figure 4. The off-axis rotational stage selects the wanted KEDF and moves its position within the field of view of the telescope; the on-axis rotational stage aligns the edge of the KEDF with the lunar terminator (boundary between the illuminated and un-illuminated hemispheres).

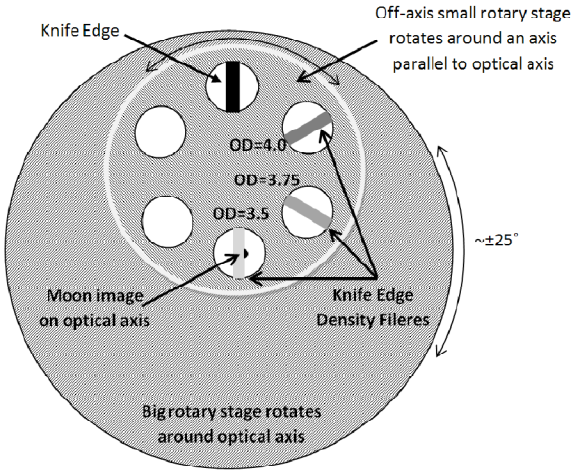

Figure 4 - The two rotary stages for the selection and positioning of the knife edges optical density filters [7].

2.2 Telescope Operational Modes

The albedo calculation requires measurements of the earthshine and bright side of the moon. Simultaneous observation of both quantities is very difficult to achieve due the huge difference between their intensities, and for this reason the sequential approach have been used historically to observe the earthshine.

The LO/DMI Earthshine telescope has 4 different operational modes named BBSO, modified BBSO, Co-Add and Lund Mode, all of them suitable to perform earthshine measurements [7]. The first two methods use the sequential observation approach, and the last two uses simultaneous observation of both sides of the Moon.

- The **BBSO mode** is named this way because it is based on the mode used by the Big Bear Solar Observatory on its earthshine telescope [2]. It is a sequential mode where the images of the bright side (BS) and dark side (DS) of the Moon are taken one after another. For the DS observation the BS is blocked using the Hard Knife Edge filter to avoid saturation of the detector.
- The **modified BBSO mode** uses the same scheme as the BBSO mode, but using a neutral optical density for the BS observations covering the complete field of view. As the BS intensity of the moon is typically 10^4 times brighter than the DS, the presence of the grey optical density will extend the needed exposure time to make it similar to the one needed for the DS observation, improving in this way the relative precision of the system. Precise characterization of the density filter is needed to maintain the accuracy of the system. This is also a sequential mode.
- The **Co-add mode** stores and consecutively adds in memory many frames with exposures near to produce saturation at the BS of the Moon image. This mode effectively decreases the Poisson photon noise at the DS of the image avoiding saturation effects at the BS.

- In the **Lund mode** KEDFs (Knife Edge Density Filters) are placed at the first image plane of the telescope to dim only the BS of the moon to have an intensity level similar to the one of the DS of the moon.

2.3 Albedo Calculation from Earthshine Measurements

Qui et al. gives in [2] a detailed explanation for the calculation of the Earth reflectivity using the radiances from reference patches in the BS and DS of the Moon obtained by integration of their brightness over their areas.

The paper defines the apparent albedo of one night as following:

$$p^*(\theta) = \frac{3}{2f_L}\frac{I_a/T_a}{I_b/T_b}\frac{p_b f_b(\theta)}{p_a f_a(\theta_0)}\frac{R_{EM}^2}{R_E^2}\frac{R_{ES}^2}{R_{MS}^2}$$

$$\text{with } f_L = \frac{(\pi - |\beta|)\cos\beta + \sin|\beta|}{\beta}$$

In the previous expressions f_L is the Earth's Lambert phase function with β the Earth's phase angle, I_a and I_b are intensities of the reference patches illuminated by the earthshine (DS) and moonshine (BS) respectively; T_a and T_b and p_a and p_b are the transmittance through the atmosphere and the physical reflectivity for both patches, respectively. The variables R_{EM}, R_{ES}, R_{MS} are the Earth-Moon, Earth-Sun and Moon-Sun distances, in that order; R_E is the radius of the Earth. The lunar phase function $f_b(\theta)$ is the normalized change in moonshine intensity as a function of the lunar phase angle θ, and $f_a(\theta_0)$ is the lunar phase function for the near retro-reflection on the patch illuminated by the earthshine, with θ_0 the biggest angle between the earthshine that is incident and reflected from patch on the DS to the telescope location (typically 1° or less). For more clarity a diagram illustrating the explained angles is shown in Figure 5.

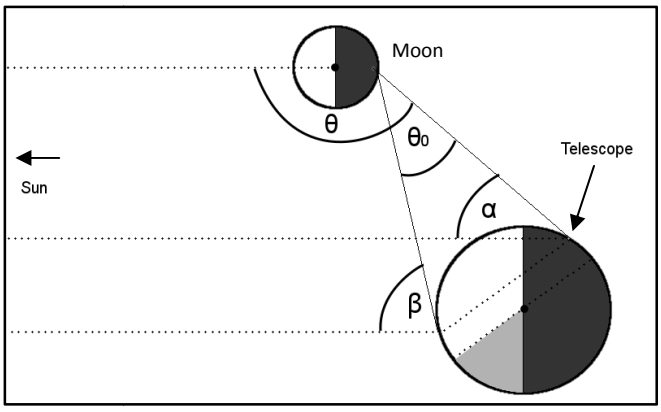

Figure 5 – Diagram showing the Moon, the Earth, and the angles used for the Earth's albedo calculations (not in scale)

The lunar phase function can be determined from Moon measurements, and the ratio p_b/p_a of the physical reflectivity of the lunar patches can be measured in a total lunar eclipse [2].

The intensities I_a and I_b are the variables to be monitored with the Earthshine telescope to obtain the apparent albedo.

To estimate the global albedo from the obtained apparent albedo, it's necessary to consider the data over all the phases of the Moon with the following integral:

$$A = \frac{2}{3}\int_{-\pi}^{\pi} d\theta\, p^*(\theta) f_L(\theta) \sin\theta$$

However, this estimation only covers an area about 2/3 of the Earth since it's based on observations taken only from one location. For this reason a network of Earthshine telescopes around the world is needed to provide realistic global albedo estimations. Combining the data from enough stations situated in different longitudes will improve the spatial and temporal coverage of the Earth's albedo estimations [3].

3. Analysis of Shutter Performance

As the calculation of the Earth´s albedo is based on the ratio between the measured earthshine and sunlit irradiances, the use of a fast shutter is essential to properly control the exposure time and to avoid the smearing effect. This is very important for all the operational modes of the LO/DMI Earthshine telescope except for the Lund Mode that only needs to take long exposures.

The present section reports the characterization of the shutter response of the Earthshine telescope. The shutter is the VS25 model from Uniblitz [8], and it has an opto-electronic synchronization system that provides an electronic signal that allows obtaining the opening time of the shutter. In order to calculate the pulse width of the synchronization pulse, a NI-6229 data acquisition card and codes running in LabVIEW were used. The input with a timebase of 80 MHz of the A/D card was used to produce precise measurements of the pulse width.

As the goal of the Earthshine project is to achieve albedo measurements with 0.1% of accuracy, estimations of the amount of precision for the exposure time measurement were also made.

3.1 Experimental Setup

Two different experiments were performed in the optical laboratory using a photodiode (Thorlabs FDS100) and a digital oscilloscope (Tektronix TDS2014B) to measure the shutter response. In both cases the light from a thermal light source was collected using the Earthshine Telescope where the CCD detector was replaced by the Thorlabs photodiode, as shown in Figure 6. The used light source was a light bulb powered by a switching-mode DC voltage source.

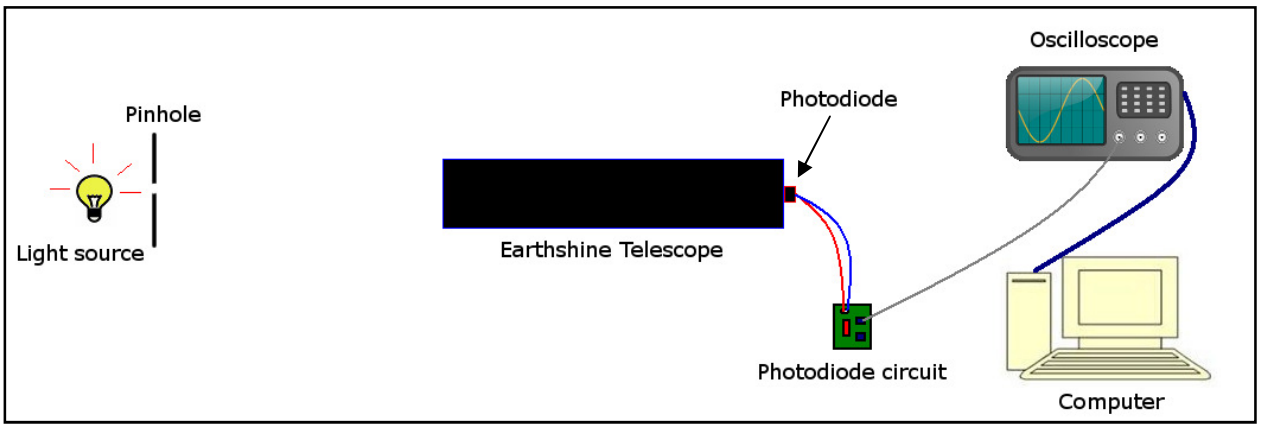

Figure 6 - Experimental setup. The shutter was tested at its operating location inside the Earthshine Telescope.

In the first experiment curves of the exposures were obtained using the photodiode while the values of the exposure times obtained with the opto-electronic synchronization system were recorded simultaneously; this was done for several exposure times in order to measure the accuracy of the synchronization system. In the second experiment 100 measurements of the same exposure time were taken with the photodiode and with the synchronization system to analyze the precision of its repeatability.

3.2 Electronic Setup

The photodiode FD100 was connected according to the recommended circuit diagram (showed in Figure 7) using a bias voltage of 20 Volts, and a load resistor R_L of 10kΩ in order to reduce the response speed and linearity of the element. The value of the resistor was chosen in virtue of existing tradeoff between signal amplitude and speed of response (for a load resistor of 10kΩ a rise/fall time of 10μs was found experimentally for the circuit, using a periodic signal in a LED as light source with a rise/fall time about 1μs).

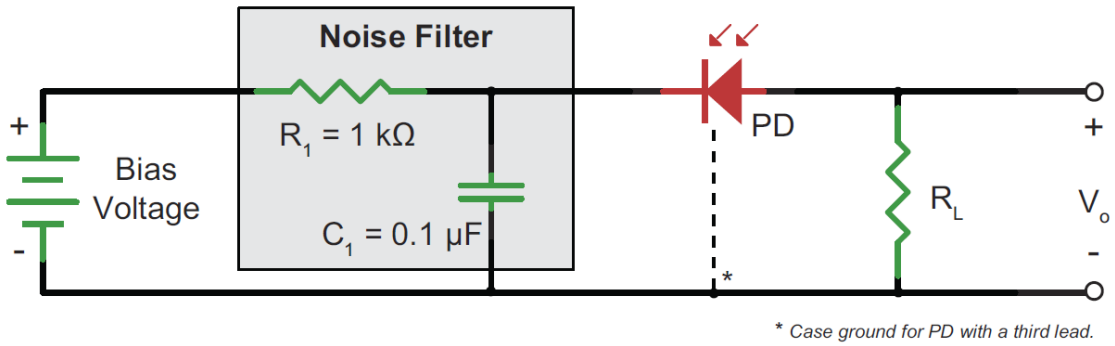

Figure 7 - Photodiode circuit diagram used (from THORLABS FDS100 Specification Sheet [9])

3.3 Calibration Curve

The photodiode output voltage was acquired with the digital oscilloscope: The NI LabVIEW *Signal Express* software was used to control it and transfer the data. The Earthshine telescope LabVIEW VI program was used to control the shutter and to record the optoelectronic synchronization output signal. To obtain the calibration curve 12 different exposure times were selected, and for each one 10 measurements were done. Examples of curves obtained with the photodiode for different exposure times are shown in Figure 8.

The telescope VI software directly gave the measured exposure time by the mechanical shutter measuring the synchronization pulse width through the NI-6229 data acquisition interface of the PXI telescope control computer. For the analysis of the photodiode signals, a MATLAB™ code was created to calculate the exposure time using the FWHM criterion for the pulse width.

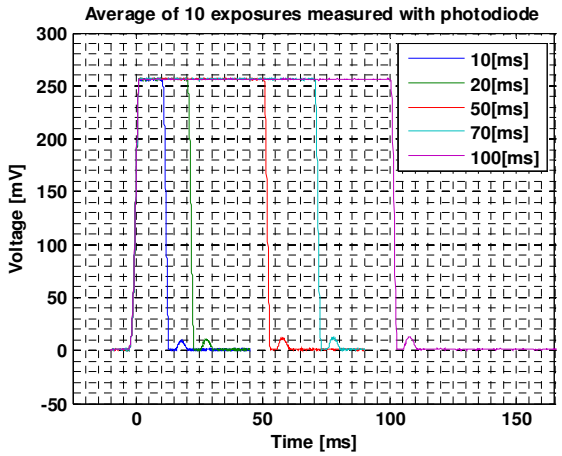

Figure 8 - Example of shutter curves obtained with ther photodiode for different exposure times

The obtained data from both, photodiode and shutter's opto-electronic synchronization system, are shown together in Table 1 and graphically in Figure 9.

Requested [ms]	Mean of exp.times from PD curves [ms]	STD of exp.times from PD curves [ms]		Sync. signal mean[ms]	Sync. signal STD[ms]	
8	**8.992**	0.017	[0.19%]	**4.7497**	0.0143	[0.30%]
10	**11.986**	0.019	[0.16%]	**7.9565**	0.0135	[0.17%]
20	**21.834**	0.019	[0.09%]	**17.7958**	0.0123	[0.07%]
30	**31.858**	0.024	[0.08%]	**27.8240**	0.0189	[0.07%]
40	**41.868**	0.019	[0.05%]	**37.8570**	0.0175	[0.05%]
50	**51.872**	0.041	[0.08%]	**47.8550**	0.0171	[0.04%]
70	**71.876**	0.035	[0.05%]	**67.8685**	0.0186	[0.03%]
90	**91.83**	0.067	[0.07%]	**87.8628**	0.0169	[0.02%]
100	**101.84**	0.052	[0.05%]	**97.8668**	0.0059	[0.01%]
150	**151.84**	0.052	[0.03%]	**147.8769**	0.0103	[0.01%]
200	**201.85**	0.053	[0.03%]	**197.8833**	0.0117	[0.01%]
220	**221.88**	0.042	[0.02%]	**217.8888**	0.0103	[0.01%]
	Average STD [ms]:	**0.037**	**[0.07%]**		**0.0139**	**[0.06%]**

Table 1 – Mean values and standard deviations of the measured exposure times obtained from the photodiode (second and third columns) and from the optoelectronic synchronization signal of the Uniblitz shutter (last two columns). Standard deviations are also shown as percentage of the mean value inside brackets.

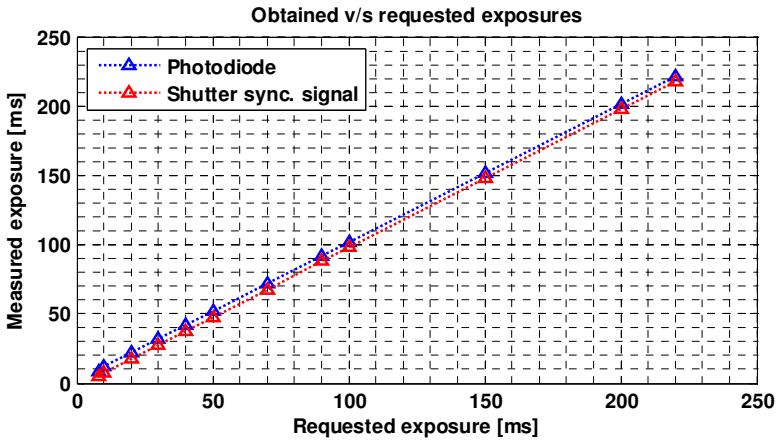

Figure 9 – Measured exposures using photodiode and shutter's synchronization system versus requested exposures.

The difference between the two measurements of the exposure times is presented in Figure 10 using error bars to indicate the quadratic addition of both standard deviations.

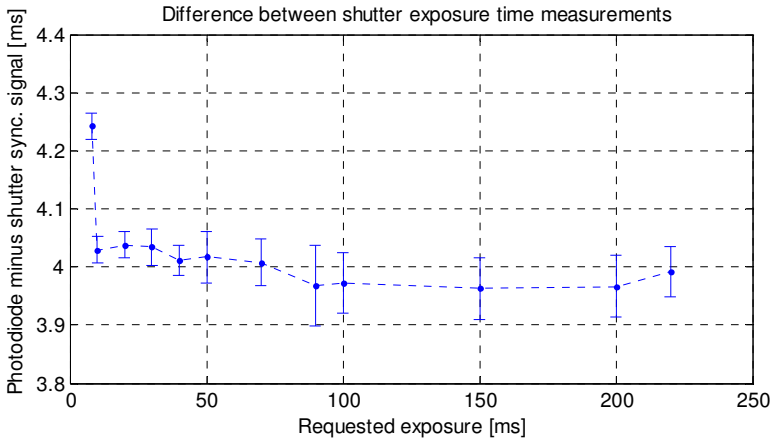

Figure 10 - Difference between measured exposure times obtained using the photodiode and the optoelectronic synchronization signal from the shutter.

It can be seen from Figure 10 that the difference between the exposures measurements increases for shorter times, and also a non-linear behavior is observed for the shortest exposures. Consequently, the linear part of the calibration curve relating the measurements from both sensors was obtained doing a linear regression excluding the 8ms data; its result is shown in Figure 11.

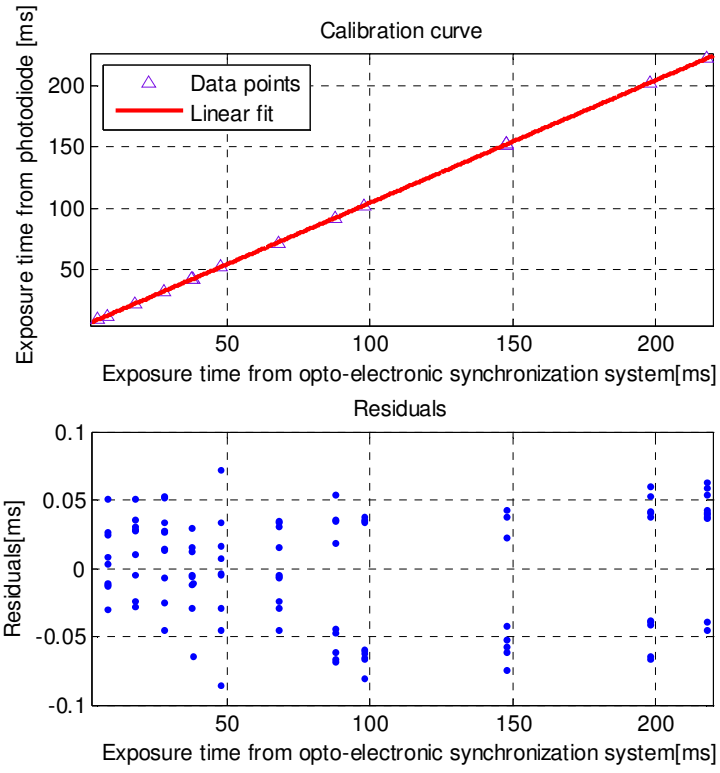

Figure 11 - Calibration curve between the measurements of the photodiode and the synchronization signal from the shutter.

The parameters obtained of the linear regression calculated in MATLAB™ are:

```
Linear model:
     f(x) = p1*x + p2

Coefficients (with 99.9% confidence bounds):

       p1 =      0.9997 ± 0.0002
       p2 =       4.028 ± 0.022 [ms]

Goodness of fit:
  R-square: 0.9999996
```

The uncertainty on the coefficient *p1* is the error in the slope of the linear calibration. It corresponds to 0.02% of the exposure, regardless its value. The uncertainty on the coefficient *p2* is an additive error showing the ambiguity in the constant level, and its importance is higher for shorter exposures. It corresponds to 0.1% of the 22ms, and is the 0.11% and 0.22% of exposures of 20ms and 10ms respectively.

3.3.1 Discussion

It was observed that there is a systematic difference between the measured values of the two sensors, and also between the requested and obtained values for both sensors. The values obtained with the shutter optoelectronic synchronization system have high precision (standard deviation ~15µs) although they present a bias of roughly 4ms. This high precision is due to the fast response of the optoelectronic synchronization system (based on the interaction between an infrared emitting diode with an infrared sensitive detecting transistor [8]) and the high sampling frequency of the DAQ card. The large bias between the two measurements is in part due to the different criteria used to determine the pulse width. While in the photodiode calculations used the FWHM criterion, the optoelectronic synchronization signal is activated only when the shutter is open more than the 80% [8]. However this effect can explains a bias up to 2ms only. A possible explanation for this large bias is that unnoticed saturation was reached in the photodiode before reaching the maximum height of the pulse; this would trim the higher part of the pulse and consecutively expand its FWHM pulse width. A future experiment will be done to clarify this matter.

The obtained linear regression for the calibration curve has R-square value very near to the unity, indicating a very good fit. The vertical dispersion observed in the residuals shown in Figure 11 is due the lower precision of the photodiode measurements compared to the precision of the synchronization system. However, as the residuals are more or less symmetrically distributed with respect the axis their effect is cancelled producing a good linear fit. As it was previously mentioned, the uncertainty in the slope of the calibration curve is 0.02% for all the exposures, and the uncertainty of the constant term is lower than 0.1% for exposures higher than 22ms. The uncertainty of the calibration is also of the order of 0.1% for the short exposures, with a maximum value of 0.22% for 10ms.

The calculated calibration curve allows the correction of the exposure values obtained with the opto-electronic synchronization system of the shutter to achieve the accuracy of the oscilloscope

measurements, eliminating any bias. Even if the repeatability of the photodiode measurements is worst, its accuracy (error of the mean value) is better because as we observed the actual shapes of the pulses we know exactly how the definition of width of the pulse is applied.

As a comment, the relative standard deviations of the photodiode measurements shown in Table 1 are not continuously decreasing for longer exposures due the change the time base of the oscilloscope needed to observe the complete width of the photodiode's pulses. The time base used were 25ms for the 8ms exposure, 50ms for 10ms to 30ms exposures, 100ms for 40ms to 70ms exposures, and 250ms for the rest; the corresponding single shot resolutions are 10µs, 20µs, 40µs and 100µs respectively.

The data measured for 8ms exposures was no considered for the calibration because it diverged from the linear tendency.

Also in the photodiode curves a small bouncing back bump after the closing was detected as we can see in Figure 8, with same characteristics for all the exposures. It will be examined in more detail in the next section.

3.4 Repeatability test

In this part 100 measurements were done for only one exposure time using the same setup as in the previous part. The selected exposure time was the minimum of the calibration curve having an error less than 0.1, corresponding to an exposure time of 30ms with a time resolution of 10µs.

As in the previous experiment, the outputs of both sensors were stored simultaneously. However only 62 of the 100 values obtained with the opto-electronic synchronization system of the shutter were valid due a problem with the electric noise filter of the system that led to 38 false detections.

3.4.1 Results

The 100 photodiode curves were averaged to produce a curve almost completely free of noise; a sample of the curve prior the averaging is shown in Figure 12 whereas the average curve is shown in Figure 13.

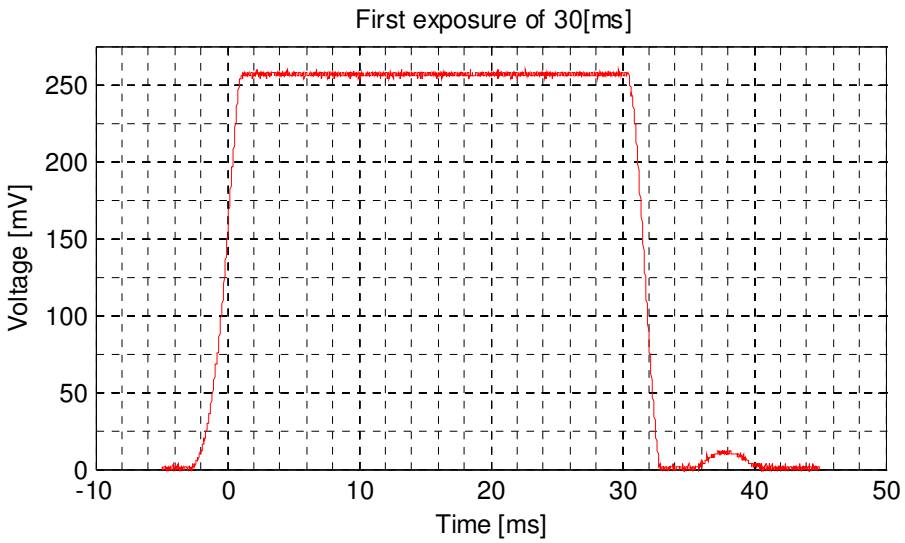

Figure 12 – Sample of curve obtained with the photodiode and oscilloscope

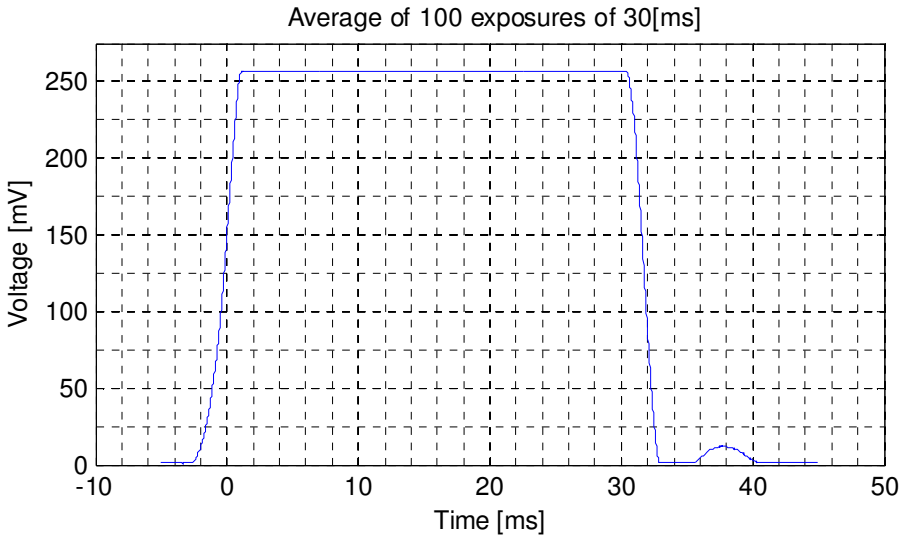

Figure 13 – Average of 100 samples obtained with the photodiode and oscilloscope

The following information was obtained from the averaged curve:

- Time duration (FWHM): 31.86[ms]
- Rise duration*: 2.22[ms]
- Fall duration **: 1.58[ms]

* measured from 10% to 90% of the maximum of the signal

** measured from 90% to 10% of the maximum of the signal

In the curve there is also visible a bounce “bump” signal of the following characteristics:

- Time duration (FWHM): 3.04[ms]
- Delay of bump maximum*: 5.22[ms]

  End time (at 10% of maximum) **: 41.76[ms]

- Maximum value: 4.6% of the amplitude of the signal
- Percentage of the main curve (ratio of areas): 0.5%

* measured from the falling edge (at 10% of the maximum of the signal)

** measured from the rising edge (at 10% of the maximum of the signal)

The statistics of the 100 photodiode curves and of the 62 outputs of the opto-electronic synchronization system are presented in the Table 2:

	Mean value [ms]	STD [ms]	STD [%]
Requested exposure time	30	-	-
Photodiode measurement FWHM (100 samples)	31.871	0.0219	0.07
Photodiode measurement FWHM (62 samples)	31.868	0.0222	0.07
Output shutter synchronization system (62 samples)	27.851	**0.0156**	0.06

Table 2 –Statistics of the exposures measured using the photodiode and the synchronization signal of the mechanical shutter. The second row shows the values obtained with the photodiode for the 62 exposures measured correctly with the opto-electronic system.

3.4.2 Discussion

The quality of the obtained curves using the photodiode was satisfactory and exposure, rising and falling times of the signal were calculated from them. The obtained exposure time has better agreement with the requested time than the output of the shutter synchronization system; however, the repeatability of the opto-electronic system of the shutter is better.

The time duration of the pulse, as well as its rising and falling times, are very stable. The only observed problem with the shutter response is the small bump after the closing originated by the bounce back of the shutter; thus it is necessary to add some delay on starting the readout process of the camera of about 10ms to remove the smearing caused by the bump. It was observed that the bump has the same characteristics regardless the value of the exposure time. For the analyzed exposure, i.e. 30ms, the integrated area under the bump corresponds to 0.5% of the main pulse area, and for the shortest exposure it corresponds to the 1.5%. This area is equivalent to 168µs of additional exposure if the photodiode response was perfectly linear and the measurements didn't suffer of any saturation effects. However this cannot be assured at this time.

Using the obtained calibration curve, it is possible to correct the bias of the opto-electronic synchronization system reducing the error to its repeatability fluctuations. The measured repeatability error of the shutter corresponds to the 0.05% of the mean photodiode exposure for 30ms, and it corresponds to the **0.13%** of the mean photodiode exposure for 10ms.

4. Analysis of Spectral performance

This section reports the characterization of the spectral response of the filters and knife edge optical densities of the Earthshine telescope and also examines the spectral response of the complete telescope.

4.1 Experimental Setup

An Ocean Optics fiber spectrometer was used to obtain the spectrum of the light through the telescope, using a halogen light source. The spectrometer was placed in the position of the CCD camera, and it was used without the fiber to increase the amount of collected light. Transmission spectra were obtained for different configurations of the Earthshine telescope in order to study the performance of each color filter, as well as of the knife edge filters. The used setup is schematically shown in Figure 14, and the main used elements are the following:

- Earthshine telescope
- Spectrometer: Ocean Optics USB2000[2] (grating groove density of 600nm^{-1}) [10]
- Halogen light source
- Circular aperture to decrease light intensity
- Computer for data acquisition (with *OOIBase32* software)

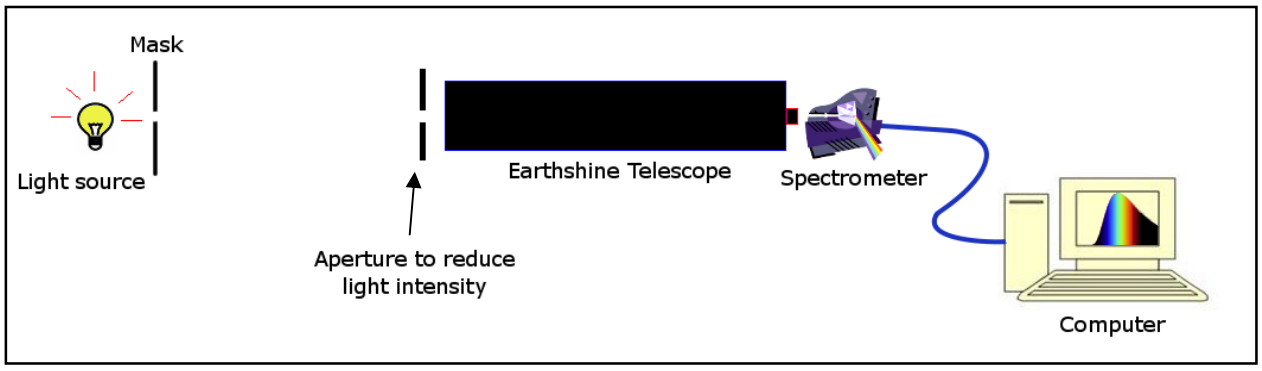

Figure 14 - Experimental setup. The shutter was tested placed inside the Earthshine Telescope.

An analysis of the non-linearity of the spectrometer was performed before the actual measurements of the spectral transmission to ensure correct results.

4.2 Analysis of non-linearity of the Spectrometer:

All CCD detectors suffer some amount of non-linear behavior on their response to the light, and CCD based spectrometers are not an exception. This non-linearity can be corrected if it is measured, and the USB2000 spectrometer has the ability to correct the acquired data using a 7th order polynomial which coefficients can be stored on its EEPROM internal memory. The *OOINLCorrect* software available in the *Ocean Optics* website allows the calculation of these coefficients doing a simple experiment. According

[2] Specifications shown in the Appendix

to the manufacturer the response without any correction of the USB2000 spectrometer is linear to 93% and linearity >99.8% can be achieved using the correction [11].

The *OOINLCorrect* software analyses the non-linearity of the detection using constant light source intensity while changing the integration time. It measures the response of 9 selected pixels across the detector that have to be selected in the way that they all reach the saturation at the higher integration time limit of the test, and also all they must start with as few as possible counts in the low integration time limit in order to cover most of their dynamic range. The selection of pixels can be done automatically or manually in the software, and their positions will determine the range in wavelength where the correction will be more effective, and also the quality of the correction. The manufacturer affirms that measurements of only 9 pixels are necessary arguing that the nonlinearity of each pixel is identical in one detector [11]. The software stores the values of count and counts per second of the 9 pixels for different integrations times, covering the interval between both integration time limits. With the combined collected data of all the pixels, the program fits a 7^{th} order polynomial in the relation between the normalized counts per second and counts, and this polynomial generates a correction factor for the pixels in function of its number of counts. The way to apply the correction is dividing the original numbers of counts by the obtained correction factor for all the pixels.

4.2.1 Calibration Procedure

The first thing to do was to find a suitable light intensity for the experiment. Using the halogen light source, saturation (i.e. 3800 counts) was reached for the pixels between 460nm and 770nm using 500ms of integration time. The stability of the used light source, which was measured with the telescope CCD camera using 100ms exposures, is shown in Figure 15; the spectrum the light source is shown later in Figure 23. The exposures times for the test were chosen in order to obtain the biggest amount of saturation at the high integration time level while at the same time produce relatively few counts at the low integration time level; the selected low integration time level for the calibration measurements was 10ms producing around 300 counts above the dark level at the higher peak of the light source spectrum.

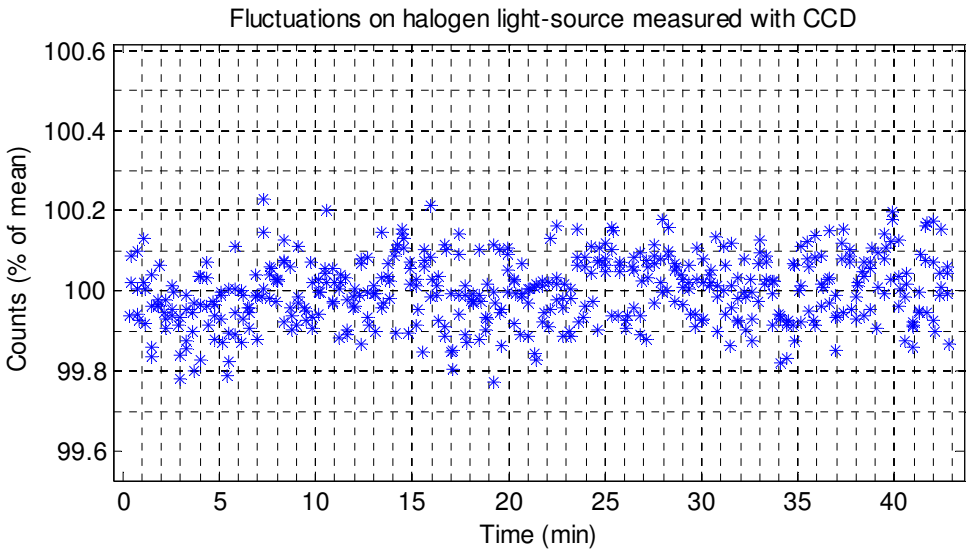

Figure 15 - Stability of the used halogen light-source measured using Andor CCD camera.

The experiment was repeated many times, testing different values for the integration time limits and for the integration incremental step. Also different pixel selections were tested. In this way many calibration polynomial candidates were obtained.

A second experiment was performed to check the quality of the candidates. Spectra of the light source were taken at different intensities changing the integration time using the *OOIBase32* acquisition software with the non-linearity correction turned off. Afterward, the candidate calibrations were applied to the data using a code in MATLAB™, and then ratios between the spectra of different integration times were calculated and normalized. The obtained ratios are correlated with the goodness of the calibration candidates, and for ideal perfect correction this ratio should be the unity for all wavelengths.

4.2.2 Results

As was previously mentioned, many similar but different calibration polynomials were obtained using the *OOINLCorrect* software. An example of Nonlinearity Correction Report is shown in Figure 16. It shows the acquired data points, the regression results of the fitted 7th degree polynomial, and the processed output after the application of the calibration.

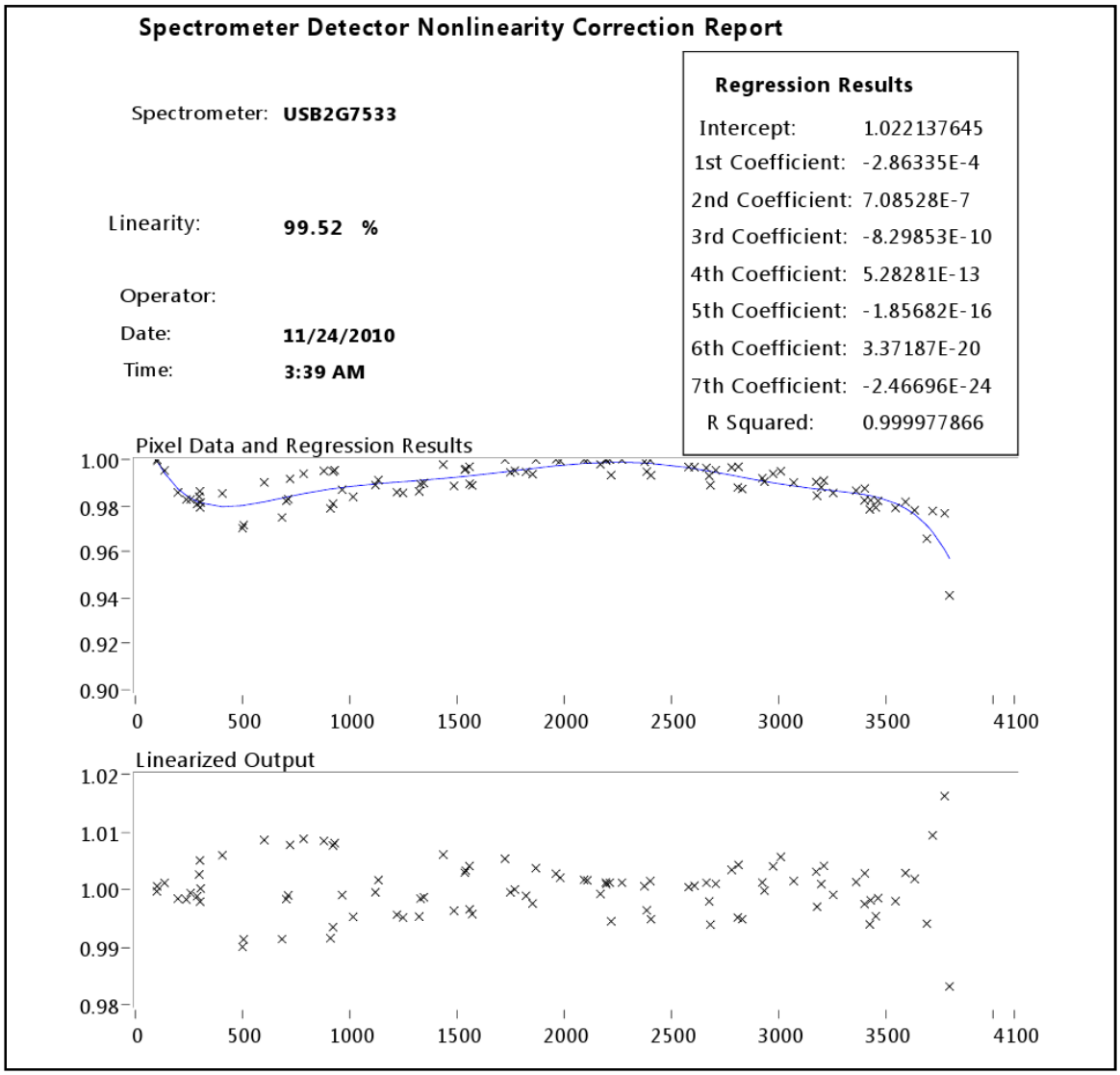

Figure 16 - Example of Non-linearity calibration report generated with the *OOINLCorrect* software. The settings for this example were high integration level of 900ms, low integration level of 10ms and integration step of 20ms. The y-axis values are the normalized counts per second. The x-axis values are the counts. This example was the best correction obtained with the software.

Unfortunately the calibration software did not produce a stable output, and many different polynomials of different characteristics were obtained repeating the procedure.

The second experiment was made to find the most suitable calibration for our purpose. It was to compare spectra of the same light-source taken with different exposures. Figure 17 shows the obtained

ratios (normalized) between a short and a long exposure for three different calibration settings: no calibration, typical obtained calibration, and best found calibration. The peak value of the spectra was 90 counts for the short exposure, and 3220 for the long exposure. The normalization was done making equals the areas under the spectra before taking the ratios.

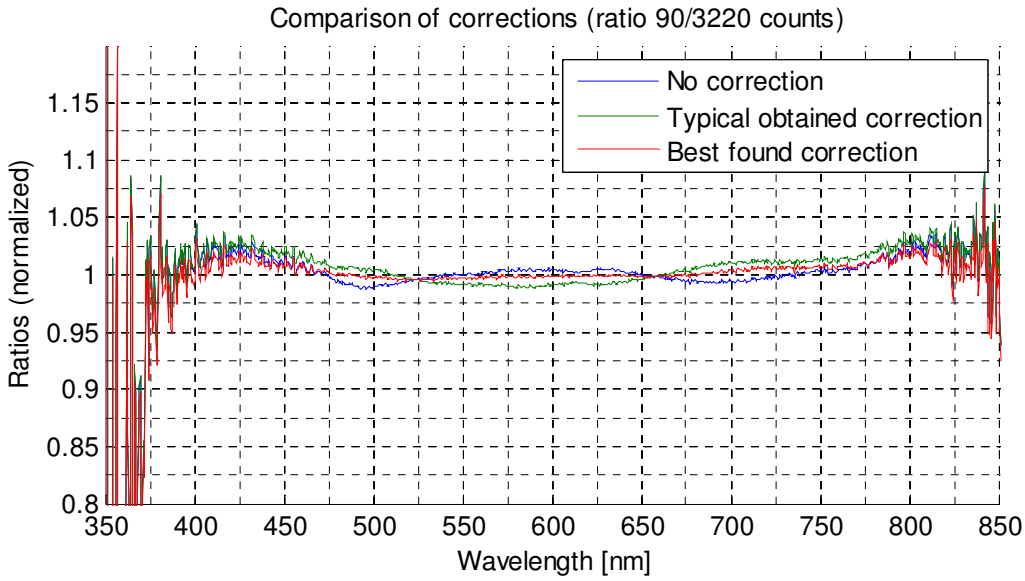

Figure 17 - Ratios between the spectra of same light source at different exposures. Ratio *90/3220* means a short exposure spectrum with a maximum value of 90 counts divided by long exposure spectrum with maximum value of 3220 counts.

The *90/3220* ratio shown in Figure 17 was the one that covered the widest dynamic range of the detector, because the spectrum with maximum at 90 counts was obtained using the minimum possible exposure in the spectrometer, 3ms. The level with maximum at 3200 counts was chosen because it was a high value but far enough of the actual saturation level (3800 counts) to avoid undesired effects; it was achieved using 100ms of integration time. The light intensity used was the same chosen for the subsequent transmittance measurements, the highest attainable intensity.

In the experiment more intensity levels were measured using exposures of 12ms, 25ms and 50ms corresponding 380, 790 and 1590 count for the maximum peak, respectively.

It was found that for the ratios for the uncalibrated data, the worst was the ratio *90/3220* as expected and shown in Figure 18.

The best calibration was obtained slightly modifying in MATLAB the polynomial of the measured candidate with better performance in the ratio test (shown in Figure 16) giving special importance to the ratio *90/3220* because the measurements of transmission using the optical densities will produce weak spectra with few counts. The ratio test result of the best correction is shown in Figure 19. The coefficients of this correction are shown in Table 3.

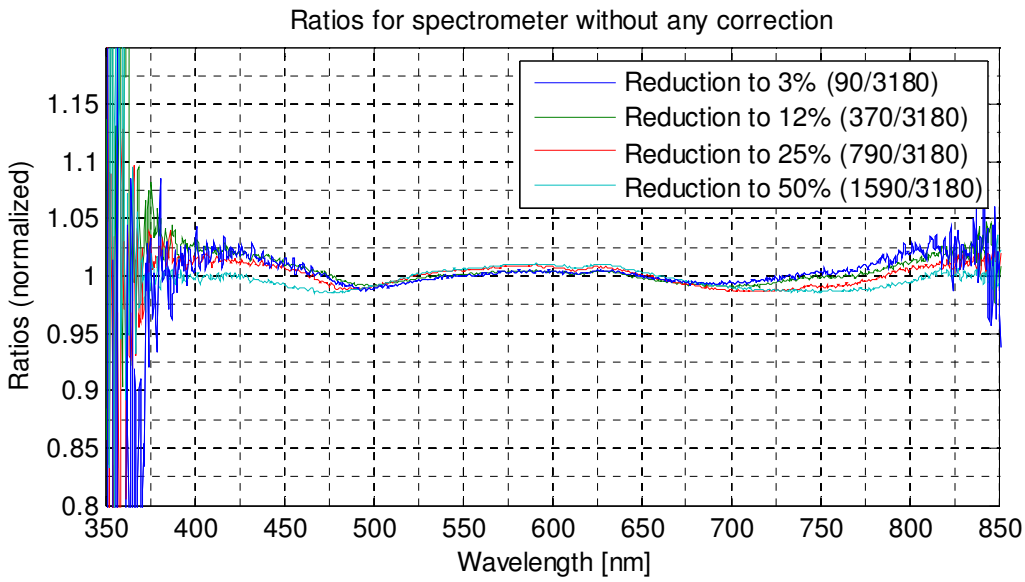

Figure 18 - Ratios between spectra of the light source at different exposures without applying any correction. The differences between the amplitudes of the spectra are also shown as percentages of reduction of the high level.

Best obtained calibration polynomial			
P0	**P1**	**P2**	**P3**
9.87098E-01	-8.67736E-05	2.74189E-07	-3.58113E-10
P4	**P5**	**P6**	**P7**
2.48280E-13	-9.35350E-17	1.79526E-20	-1.37379E-24

Table 3 - Best obtained correction polynomial coefficients: P0 is the constant term; P1 is the term associated with first power of x, and so on. The input of the polynomial is the number of counts of a pixel, and the output is the correction factor needed for that pixel.

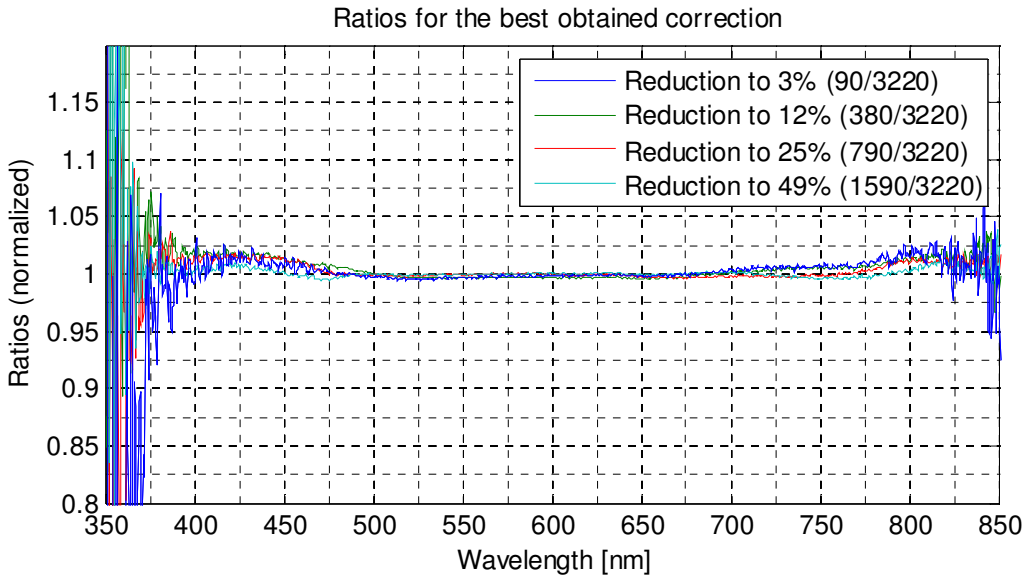

Figure 19 - Ratios between spectra at different exposures of the light source applying the best obtained correction. The differences between the amplitudes of the spectra are also shown as percentages of reduction of the high level.

Table 4 summarizes the data shown in Figure 18 and Figure 19 in terms of percentages of estimated linearity per wavelength interval. Those values were calculated using the average trend of the curves discarding the contribution of the high frequency noise peaks.

Interval [nm]	Uncalibrated	Calibrated
400 to 830	96%	98%
470 to 750	97%	99%
500 to 700	98%	99%

Table 4 – Percentages of estimated linearity

The same data from Figure 18 and Figure 19 was rearranged in function of the counts of the high level spectrum, using the spectral data of that level to associate wavelengths to counts. This led to Figure 20 and Figure 21.

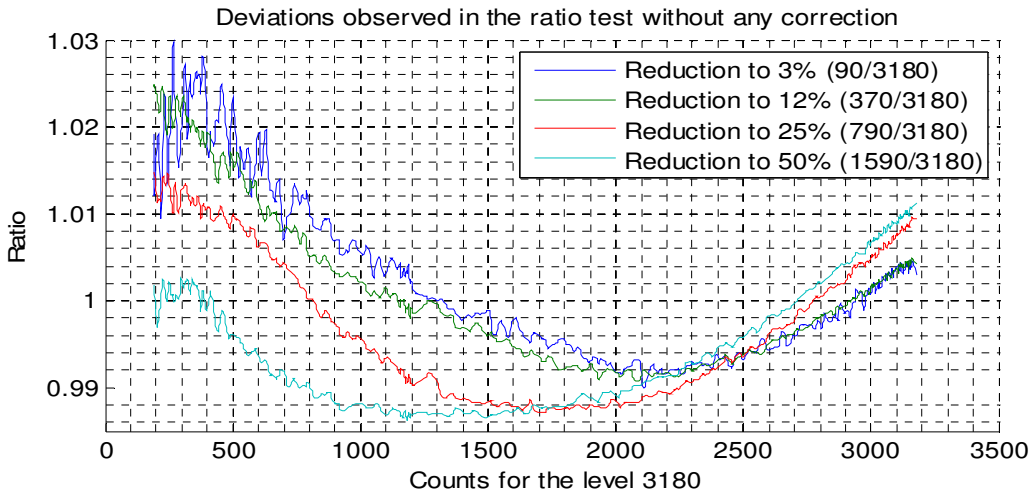

Figure 20 – The data from Figure 18 rearranged using the collected spectra to obtain this plot of ratios versus counts for the uncalibrated data.

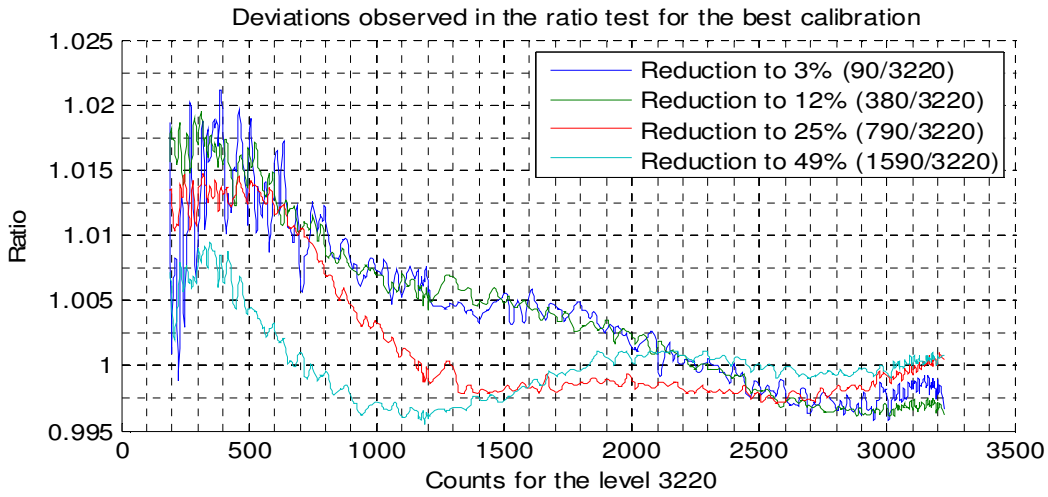

Figure 21 - The data from Figure 19 rearranged using the collected spectra to obtain this plot of deviation versus counts for the best calibration. Note that the high level slightly changed its counts from 3180 to 3220 due the calibration effect.

4.2.3 Discussion

As the knife edges density filters will reduce the intensity of the light through the telescope about 3 or 4 orders of magnitude, it is very important that response of the used spectrometer be as good in order to get reliable transmission spectra. Hence, a calibration of the response of the spectrometer to the light was performed.

Non-linearity calibration polynomials for the spectrometer were obtained using a computer program provided by the manufacturer. However the resulting polynomials showed significant variations.

One reason of this variability in the polynomials was the use of different settings in the software, specially the pixel selection. Another explanation can be changes in unmonitored the experiment variables like small fluctuations in the light source intensity or change in the spectrometer CCD detector temperature. Also the photon noise could be an important factor that affected the measurements for the low intensity measurements.

The data of the second experiment was used to determine which calibration produced a better response analyzing the result of each calibration at different intensity levels. The comparison between the highest and lowest levels (i.e. ratio *90/3220*) is of special interest because it covers the levels needed to measure the optical densities of the Earthshine telescope, and great improvement was achieved for this ratio (from 3% to 1% of deviation from linearity in the range 470nm to 750nm).

The results in Table 4 show the improvement in linearity considering all the ratios between different levels. Basically the error is reduced to its half. However there is another benefit of the obtained calibration. Comparing Figure 18 and Figure 19 we can observe that the shapes of the calibrated ratios are more planar and more similar among themselves, and this will produce more reliable spectral shapes.

The shapes of the curves in Figure 20 and Figure 21 show more clearly the effect of the calibration. The original performance of the spectrometer show non-linear behavior through all the counts range. After the calibration the non-linear behavior is strongly reduced for the higher part of the dynamic range of the spectrometer. This means that for transmittance measurements the linearity will be better for the regions where the reference light-source has higher counts; it will be better than 99% for regions with more than 1000 counts at the reference. Figure 20 and Figure 21 also show that the ratios for the highest counts are closer to the unit if the calibration is used, indicating that the used normalization criterion of equal areas and the criterion of normalization using the maximum values are more consistent.

As the calibration of the spectrometer was performed offline applying the correction to the spectra using a MATLAB code, further improvements to the non-linearity correction can be done to increase the accuracy of the spectral measurements. This improvement could be done using a different light source with wider spectrum, or modifying manually even more the obtained polynomial using MATLAB checking the result with the intensity ratio test.

4.3 Spectral measurements

Spectra of light thought the telescope were acquired using the setup shown in Figure 6, for different configuration of telescope: clear window (no filter applied), color filters and knife edge filters. The tested color filters were: JOHN-V-25, JOHN-B-25, Shortpass filter 750nm, Longpass filter 750nm; all from *Asahi Spectra Co* [12]. The tested knife edges density filters have nominal optical densities 3.5, 3.75 and 4 and were manufactured by *Ferroperm Optics A/S* [13] specifically for the Earthshine Project.

In addition, the spectrum of the light source was also measured without the telescope to examine the transmittance spectral curve of the complete telescope (losses introduced by the lenses).

4.3.1 Procedure

Before the test, the positions of the filters and knife edges were checked with the CCD camera. The telescope control software was configured to be capable of cover completely the field of view with coated part of the knife edges density filters.

First of all, the light source and spectrometer were turn on and one hour was waited to obtain stabilization of temperature in both devices. This was checked in the spectrometer monitoring the stabilization of the dark level.

Secondly, spectra of the clear window were taken using a small aperture placed in front of the telescope in order to reduce the light intensity. Spectra were acquired using the following settings: 3ms and 2000 samples averaged, 12ms and 500 samples averaged, and 100ms and 100 samples averaged to obtain maxima values of 300, 600 and 3500 counts respectively. These spectra were used to check the calibration.

After that, the small aperture in front of the telescope was removed and the reference spectrum of the clear window was measured using 7ms of exposure and 1000 samples averaged obtaining maximum about 3200 counts including dark. The experiment had to be repeated afterwards to measure the OD3.75 that wasn't available at the first time, and in this second opportunity the maximum of the reference was near 2990 counts. The dark level was about 200 counts in both occasions.

Next the spectra of the knife edges were acquired using 4s of exposure and 10 samples averaged. This produced about 750, 500 and 350 counts at the peak for the OD3.5, OD3.75 and OD4 respectively. References were taken repeatedly to check for variations in the light-source.

Later, the spectra of the color filters were measured using 7s of integration time and 1000 samples averaged.

Finally, the spectrum of the light source was measured directly, without the telescope, using 4s of exposure and average of 10 samples. This produced a spectrum with maximum about 2000 counts including the dark contribution.

4.3.2 Results

The spectral measurements of the light source using the attenuator were done to test the non-linearity calibration at the condition used for the transmittance measurements. The integration times were selected to obtain similar count values to ones obtained with optical densities of the knife edges, and ratios were calculated again between these spectra of same shape but different counts levels. Figure 22 shows the measured deviations using the chosen calibration.

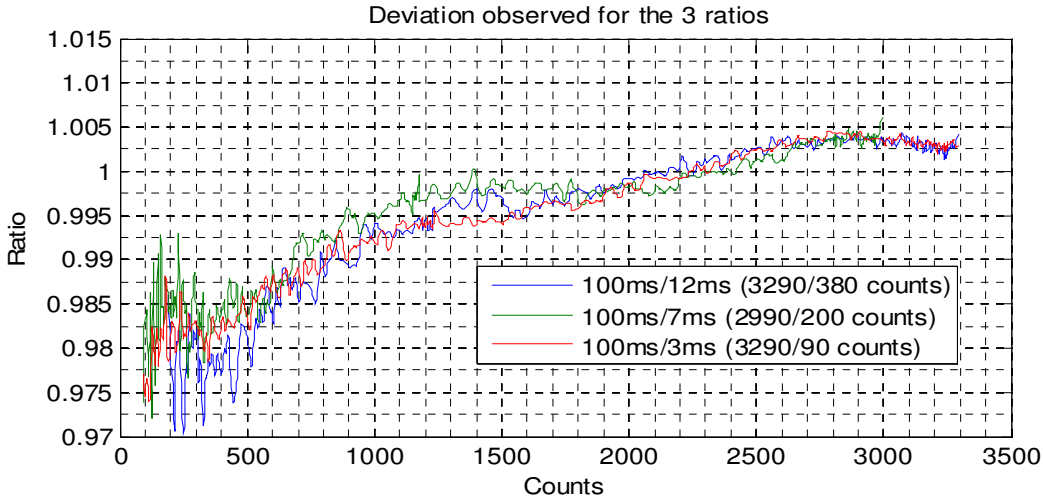

Figure 22 – Deviations obtained for ratio between levels high number of counts and count level similar to the expected for the optical densities of the knife edges

The deviation curves are consistent with the previous calibration results, and they could be used to correct even more the measurements, and it effect was tested. However the result of this new correction only shifts the resulting curves about 0.01 OD in some areas. As this new correction didn't shown any appreciable improvement in the transmittance curves of the knife edges, it wasn't considered in the measurements of the filters.

The transmission of the color filters was obtained using the measured spectra amplified by their exposure times, and then calculating the ratios between the spectra of each filter and its amplified reference. The obtained transmission curves are show in Figure 25, Figure 26, Figure 27, and Figure 28, indicating with red the discarded part. This discarded zone was not reliable because the intensities of the sample and the reference were both small together (sample less than 5 counts and reference less that 100 counts) or because the reference was too weak (less than 5 counts).

The transmission curves of the knife edge are presented in Figure 29, Figure 30 and Figure 31 as optical densities (i.e. logarithmic scale). The spectrum of the light source used for the experiment is shown in Figure 23.

The estimated spectral shape of the transmission through the Earthshine telescope with no filters is shown in Figure 24. The 100% transmission level is arbitrary in this case, and the data above 800nm was discarded because it suspicious rising behavior.

Full size plots of the obtained transmission curves of the filters can be found in the Appendix.

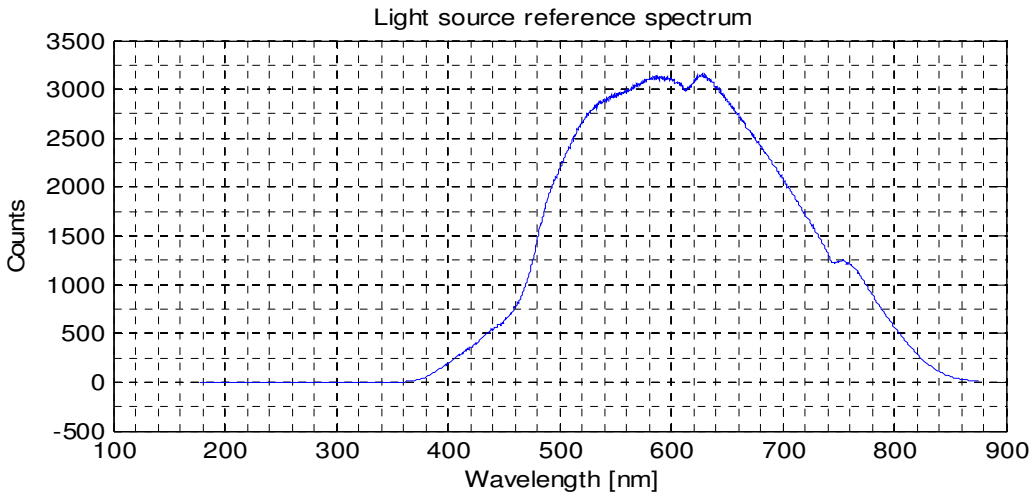

Figure 23 – Spectrum of the halogen light source used as reference for the transmission measurements and in the calibration.

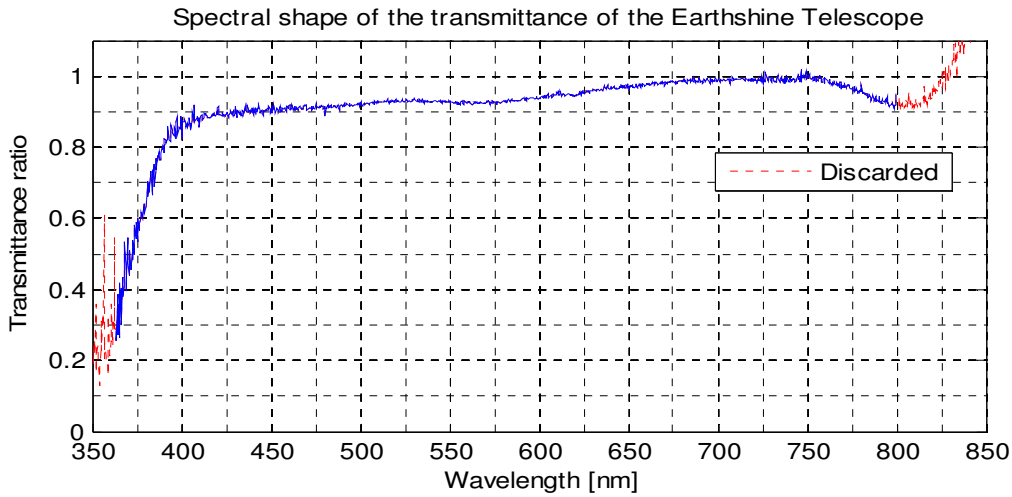

Figure 24 – Estimated spectral shape of the transmittance of the Earthshine telescope with no filters.

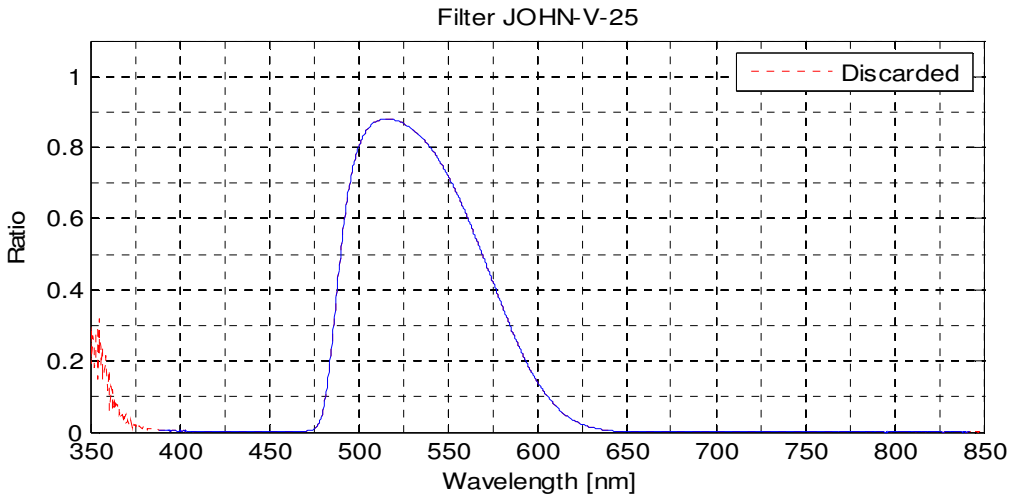

Figure 25 – Spectral transmittance of the JOHN-V-25 filter.

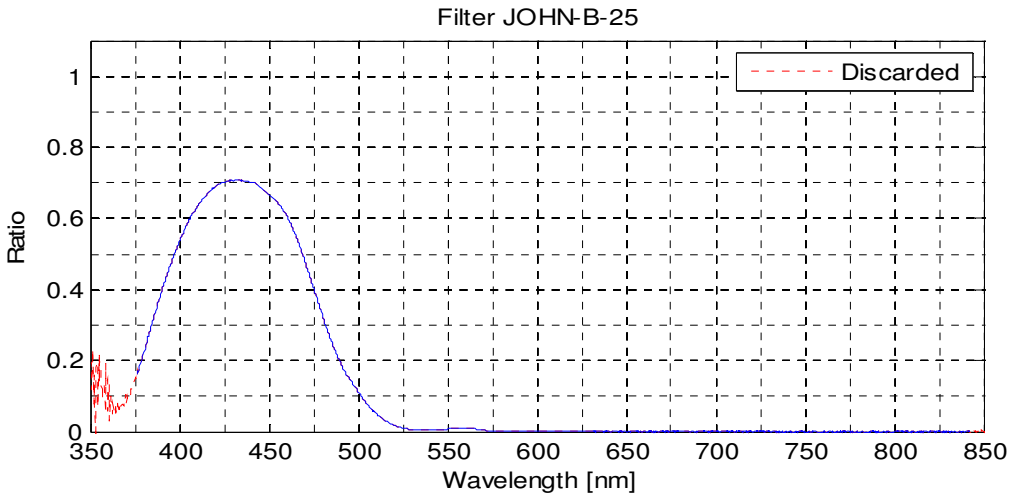

Figure 26 – Spectral transmittance of the JOHN-B-25 filter.

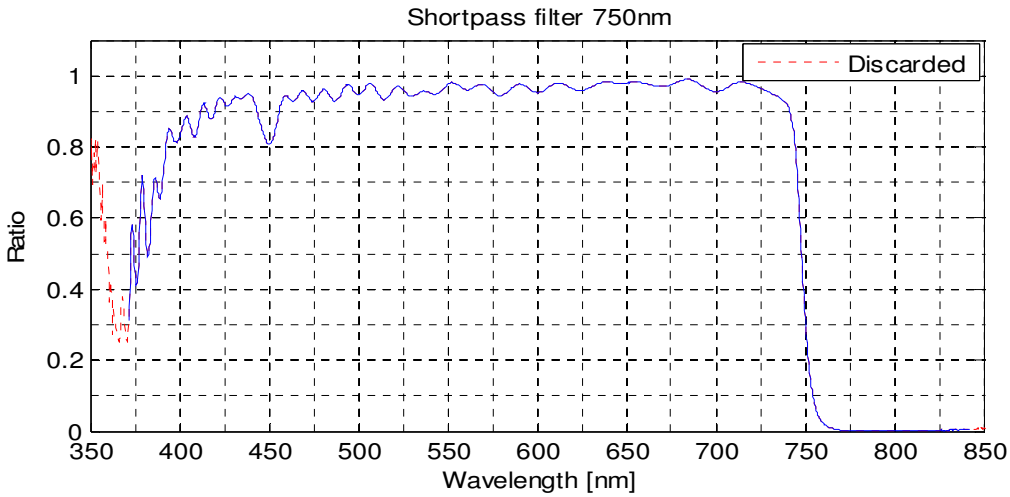

Figure 27 – Spectral transmittance of the Shortpass filter.

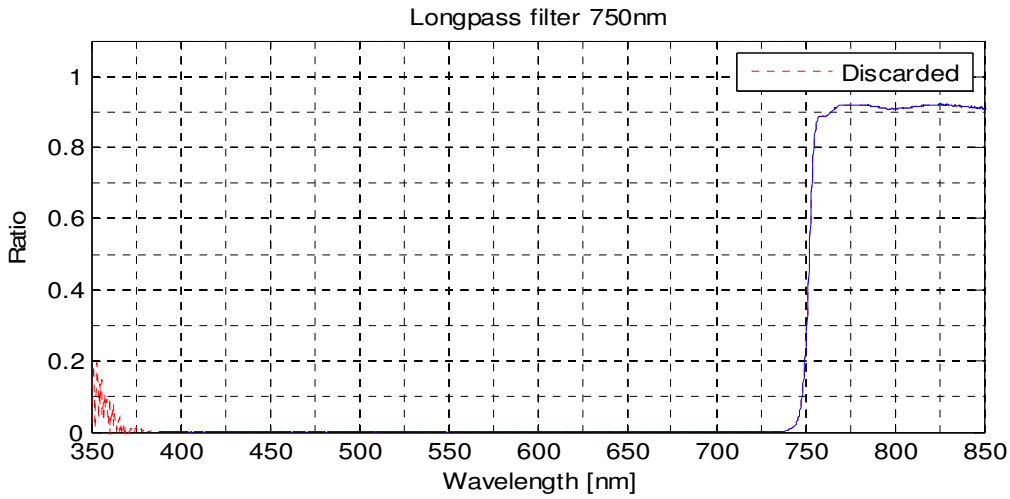

Figure 28 – Spectral transmittance of the Longpass filter.

Figure 29 – Spectral transmittance of the knife edge OD=3.5 covering all the field of view.

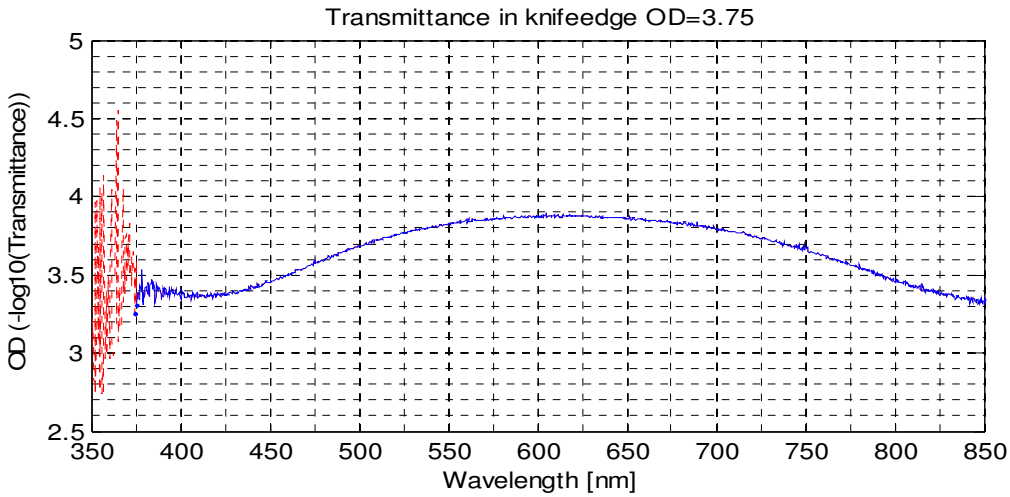

Figure 30 – Spectral transmittance of the knife edge OD=3.75 covering all the field of view.

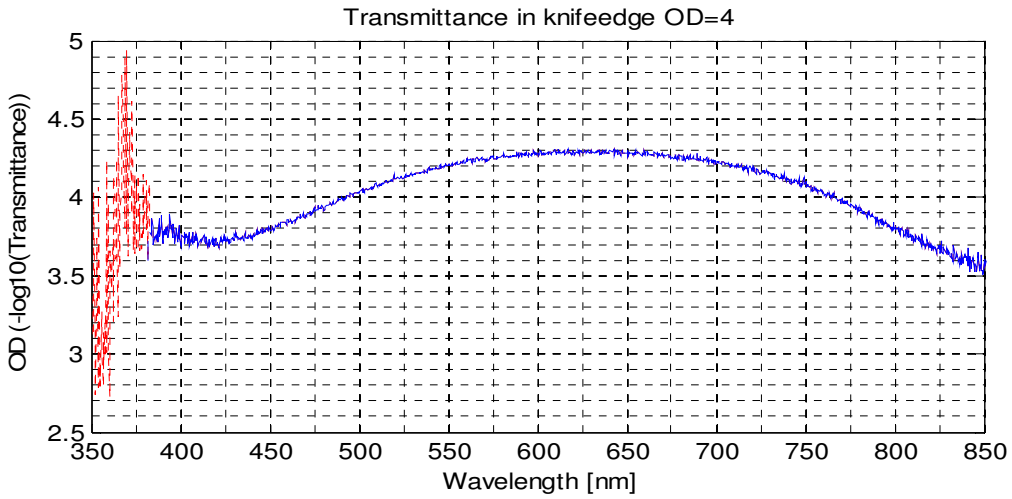

Figure 31 – Spectral transmittance of the knife edge OD=4 covering all the field of view.

4.3.3 Discussion

The obtained transmittance curves were compared with the provided by the manufacturers of the filters. The match is near perfect for the shapes and the values for the color filters. For the Shortpass filter the absorption peak near located at 450nm in the measured transmittance seems to be shifted few nanometers in the manufacturer datasheet; also the few values below 375nm seems to be over estimated.

For the knife edges the situation is different. The measured spectral transmittance of the knife edge with OD=3.5 is very different from the specified by the manufacturer, because it shows a rather planar zone from 375nm to 700nm that is not present on the manufacturer datasheet. This result was verified doing a second measurement with a different sample of the same KEDF, obtaining the same spectrum. However, the measured transmittance curves of the other two knife edges are very similar to the specified, with the difference that the measured curves seem to be slightly narrower, compressed from the right side 40nm approximately.

The differences between the measured data and the manufacturer data sheets can be described as following. For the differences observed in the color (Shortpass) filter, the most probable is that the obtained linearity exhibited in Figure 21 is not good enough for low count levels, and this will be especially important at the wavelengths where sample and reference have low but different counts levels (see Figure 23 and Figure 27). This could be improved using a better light source with more radiation towards the UV region, or enhancing the calibration reducing even more the non-linearity.

The result showing the transmission through the Earthshine telescope without any filter is the mostly a qualitative result. Because of the difficulty in measuring the absolute light level of light source itself and through telescope the transmission curve has been scaled to 100% at maximum transmission. It shows a transmittance above 90% for all the wavelengths above 450nm, and a decrease transmission going to shorter wavelengths leading to a strong reduction in the UV region as expected due the anti-reflection coating on the telescope lenses.

The transmission of the JOHN-V filter is mainly between 480nm and 600nm, with maximum value of 89% at 516nm and its FWHM is 84nm. Its transmission is mainly in the green and yellow color ranges of the visual spectrum.

The transmission of the JOHN-B filter is for smaller wavelengths, mainly between 370nm and 500nm. Its maximum transmission is 71% at 432nm, and its FWHM is 91nm. Its transmission is mostly complementary to the one of the JOHN-V filter, mainly in the violet and blue color ranges.

The Shortpass filter is broadband, with transmission higher than 80% between 393nm and 744nm. It has a sharp cut off frequency at centered at 748nm, and its transmittance is lower than 2% for wavelengths higher than 761nm. Its spectral shape has many fringes, and the biggest one is located at 450nm. Basically this filter allows the transmission of the visual spectrum, blocking the infrared component.

The Longpass filter is the complementary to the Shortpass, with a sharp cut-off frequency centered at 752nm. Its transmission is higher than 88% for wavelengths longer than 757nm, and shorter than 2% for wavelengths shorter than 744nm; its shape has not as many fringes as the Longpass filter. This filter only allows the transmission of infrared light.

The spectral shapes of the KEDF are much softer. Instead show rather sharp spectral features, they exhibit slow tendencies to absorb more between 550nm and 700nm for the optical densities 3.75 and 4, and between 650 and750 for optical density 3.5. The difference between the maximum and minimum transmission is approximately one optical density for all the KEDFs.

5. Conclusions

Different experiments were performed to measure the performance of the shutter system and the spectral performance of the color and knife edge optical densities filters of the LU/DMI Earthshine Telescope, with the objective of evaluate their contributions to the final photometric performance of the Earthshine telescope. The design of the telescope envisaged accuracy about 0.1%, and the experimental data was used to verify if this predicted accuracy was reached.

5.1 Shutter performance

The shutter system of the Earthshine Telescope was tested and characterized using a photodiode on the image plane together with an oscilloscope to observe the shape of the exposures. The data obtained from the photodiode was compared against the data of the opto-electronic synchronization signal of the shutter.

It was found that the data from synchronization signal of the shutter has good repeatability but not good accuracy. A calibration curve was obtained using measurements taken with a photodiode and an oscilloscope to correct this limitation. Using this calibration, the estimated error in the shutter measurements for the main pulse (without consider any bounce) is 0.13% at most.

A bump created by bounce of the shutter on its closing stage was detected in the analysis of the photodiode curve. The repeatability analysis showed that the characteristic of the bump, as well as the ones of the main pulse, are very stable. Thus corrections are possible to be made to include the effect of the bump in the exposures.

One way of dealing with the presence of the bump is to delay the readout in the CCD to avoid the smearing effect, producing a small over-exposure (the bump) that could be considered doing a new calibration. If the presence of the bump is not considered within a new calibration, the estimated error for the worst case (10ms) is 1.5%. Nevertheless, the effect of the bump in the data is lower than 0.1% for exposures longer than 150ms. The effect of the presence of the bump on the image exposures will be studied in a future photometric analysis of the CCD camera plus shutter system.

As the bias difference between the values of the shutter's opto-electronic synchronization system and the requested exposure is about 2.15ms and the desired error limit is 0.1%, the obtained calibration is only needed for exposures shorter than 200ms. Longer exposures will have error less than 0.1% without corrections. It has been decided that in science operation the Earthshine Telescope will use the opto-electronic synchronization of the shutter for exposures shorter than 1s and will use the requested values for the longer exposures.

The obtained linear calibration is not valid for exposures lower than 10ms. A different calibration curve is needed to properly describe the relation between the output of the shutter synchronization system and the measurements taken with the photodiode for exposures between 8ms and 10ms. Additional measurements using exposures in between are needed to produce an accurately characterization of this non-linear zone.

The standard deviations of the shortest exposures analyzed, 8ms and 10ms, are higher than 0.1% for both measurements. For the photodiode measurements this is because of their single shot resolutions that were 0.13% and 0.2% respectively although the obtained error for the 8ms exposure was 0.19%. This indicates that the error in the mechanical shutter repeatability is bigger than 10µs agreeing with the value of 16µs for the standard deviation of the output synchronization system obtained in the repeatability test.

The error in repeatability of the output of the synchronization system has two main sources. One error source is the actual fluctuations in the mechanical shutter response caused by temperature and voltages fluctuations. Another possible source of error is lack of precision on the output synchronization system measurements. The synchronization system of the shutter is a solid-state opto-electronic system that uses an infrared emitting diode, an infrared sensitive transistor and an interrupting vane [8]. The specifications of the shutter states that *Fairchild* components QEE113 and QSE114 or equivalents are used respectively as IR emitter and IR detector, having times of response about 1µs and 8µs according to their datasheets. As the output of the infrared sensitive transistor was measured using an 80MHz A/D acquisition card, enough temporal resolution was used. Therefore the observed error in repeatability is most likely originated by fluctuations on the shutter response.

The fact that the repeatability error of the output of the synchronization system is caused by the shutter itself determines that it will not affect the accuracy of the Earthshine telescope measurements because the feedback from the synchronization signal of the shutter will be used to update the requested exposure time in science operation for short exposures.

To summarize, the error in the shutter measurements is determined by the repeatability error of the synchronization system and the error of the linear calibration. The sum of both errors is 0.4% for the minimum considered exposure (10ms), 0.13% for 30ms, and less than 0.1% for exposures longer than 40ms. There is also a bias generated by the bounce of the shutter, but its effect will be removed with the photometric calibration of the CCD plus shutter system.

5.2 Spectral performance

The spectral transmittance of all the color filters and knife edge density filters (KEDF) of the LU/DMI Earthshine Telescope were measured using the USB2000 spectrometer. A non-linearity calibration was done for the spectrometer prior to the spectral measurements to reduce its associated error. Experimentally was determined that the original linearity of the spectrometer was 96%, and it was increased to 98%. Furthermore 99% of linearity was achieved with the calibration for the wavelength range between 470nm and 750nm.

The non-linear calibration was obtained after testing different candidates, selecting the one that produced best performance taking in consideration that the calibration needed to be valid for a high dynamic range in order to get reliable spectra of the KEDFs. The 98% of linearity was attained even for a reduction to the 3% of the reference spectrum.

It was found a great agreement between the measured transmission spectra and the filters specifications. The only filter that shows a discrepancy with the manufacturer datasheet was the KEDF

with optical density 3.5. The measurement was repeated using another sample of the same filter, and the same spectral curve was obtained. As the spectral curves of the others KEDF exhibit good agreement with the specifications, probably the coating process suffered some modification.

The knowledge of the shape of the KEDF spectra is important because it is needed to correct its effect on the observations of the bright side of the moon. If it is not considered, the spectral-photometric data collected using the Lund Mode will be strongly biased.

In contrast, the spectral curves of the color filters are needed for all the modes of the Earthshine telescope, to produce accurate spectral-photometric measurements.

Different information about the Earth's albedo can be extracted using the available color filters. The cut-off frequency of the filters Shortpass and Longpass is near to the "vegetation red edge" present in green vegetation [3], thus these two filters can be used to measure a vegetation index that can provide information about the percentage of vegetation present in the Earth's albedo. Also the JOHN-B and JOHN-V filters could be used to monitor the amount of reflection in the oceans present in the Earth's albedo.

Concerning the spectral shape of the whole Earthshine telescope, it mainly shows that it has low transmission below 400nm in the UV region. This was expected because the VIS-NIR anti-reflection coating applied on the telescope lenses, which is designed to have optimum transmission at the visible and near infrared regions but not for the ultraviolet.

About the accuracy of the measurements, the results of the tests comparing spectra of the light-source at different exposures show that the obtained non-linearity for transmittance measurements is 2% for all the wavelengths, and 1% between 470nm and 750nm. The stability of the used light-source was about 0.4%.

5.3 Final comments

From the analysis of the shutter response, it was found that the error was 0.4% for 10ms of exposure, and that at least 30ms are needed to obtain an error of 0.1%. The BBSO mode and the Co-Add mode of the Earthshine telescope require short exposures for the observation of the BS of the Moon to avoid saturation in the CCD camera. The optimum exposure value to observe the BS with the telescope depends on the lunar phase, but it is about 9ms.

Even though an error of 0.4% has the same order of magnitude that 0.1%, it's desirable to reduce the error for this two operating modes of the telescope. A way to achieve this, without changing the shutter, is decreasing the amount of collected light of the telescope, either reducing the aperture of the telescope or using a precisely characterized neutral density filter. If the intensity of the light is reduced 4 times, the accuracy of 0.1% will be obtained. This reduction is equivalent to use an optical density of 0.6.

It is worth noting that the Lund Mode is not limited by the shutter response, because it uses relatively long exposures. And also the modified BBSO mode will be less affected, depending on what value of optical density is used.

About the spectral characterization of the filters, the 1% of accuracy reached is enough for the spectro-photometric analysis of the albedo for all the operating modes of the telescope. However for the Lund Mode it is needed a more precise measurement the transmittance of the KEDFs, which also includes an analysis of the spatial uniformity of the filters. This is needed because the KEDFs are located in the first image plane of the telescope, thus the uniformity of the filters will be reflected on the acquired images, and this analysis must have an accuracy of 0.1%.

Acknowledgement

This thesis would not have been possible without the support of many persons involved in the different stages of the project.

I would like to thank in the first place my supervisors, Ahmad Darudi and Torben Andersen, for giving me the opportunity to work in such a great environment, and for the help and knowledge provided through all the duration of the thesis.

I am very grateful for the kind support given by Mette Owner-Petersen, especially for her invaluable comments on my thesis draft and her excellent tips to improve it.

I would also like to thank Dave Taylor and Torbjörn Wiesel for their willingness to help me, when I interrupt them to ask some questions.

I am very thankful for the generous financial support granted by the Erasmus Mundus scholarship, which made possible my participation on the Master in Photonics programme here in Sweden.

I would like to show my gratitude to Cristina Cachada for her selfless help to find mistakes in the report.

The most special thank you is for my family (Jeannette, Natalia, Orlando and Elvira) that their unconditional love helped me to overcome the difficulties and made me feel always near home.

6. References

[1] N. Oreskes, "The scientific consensus on climate change", *Science*, vol. 306, no. 5702, p. 1686, 2004.

[2] Qiu, J., Goode, P.R., Palle, E., V. Yurchyshyn, J. Hickey, P. Montañés-Rodriguez, M.C.Chu, Kolbe, E., Brown, C.T. and Koonin, S.E., "Earthshine and the Earth's albedo I: Earthshine observations and measurements of the lunar phase function for accurate measurements of the Earth's Bond albedo", *J. Geophys. Res*, vol. 108, no. D22, 2003.

[3] Thejll, P., Flynn, C., Gleisner, H. and Mattingly, A., "Earthshine: not just for romantics", *Astronomy & Geophysics*, vol. 49, no. 3, pp. 3.15-3.20, June 2008.

[4] Trenberth, K., Fasullo, J.T., Kiehl, J., "Earth's Global Energy Budget", *Bull. Amer. Meteor. Soc.*, no. 90, pp. 311–323, 2009. Permission to use the figure is granted by the AMS Copyright Notice (http://www.ametsoc.org/pubs/cr_2009.html).

[5] Hanner, M. S., Giese, R. H.,Weiss, K. and Zerull, R., "On the definition of albedo and application to irregular particles", *Astron. and Astrophys.*, vol. 104, no. 1, pp. 42-46, 1981.

[6] Owner-Petersen, M., Andersen, T., Ardeberg , A., Thejll, P. and Gleisner, H., "The Earthshine Telescope Project ", *Proc. SPIE 7012*, 70122L, 2008.

[7] Darudi, A., Owner-Petersen, M., Thejll, P., Gleisner, H., Taylor, D., Ale-Ebrahem, M., Andersen, T., "The Robotic Earthshine Telescope", *Proc. SPIE 7733*, 77332V, 2010.

[8] Vincent Associates UNIBLITZ. Shutter Products Comparison Specifications - Retrieved August 2010. [Online]. http://www.uniblitz.com/resources_filelibrary/comparisonspec_2-29-08.pdf

[9] Thorlabs, Inc. Thorlabs FDS 100 Specification Sheet. Retrieved June 2010. [Online]. http://www.thorlabs.com/Thorcat/0600/0637-S01.pdf

[10] Ocean Optics. USB Optical Bench Grating Options - Retrieved December 2010. [Online]. http://www.oceanoptics.com/Products/bench_grating_usb.asp

[11] Ocean Optics. OOINLCorrect Loading Non-Linearity Correction Coefficients Instructions - Retrieved October 2010. [Online]. http://www.oceanoptics.com/technical/OOINLCorrect%20Linearity%20Coeff%20Proc.pdf

[12] Asahi Spectra USA Inc. Astronomical Filters - Retrieved December 2010. [Online]. http://www.asahi-spectra.com/opticalfilters/astronomical_filter.htm

[13] Ferroperm Optics A/S. Ferroperm Optics A/S Website - Retrieved December 2010. [Online]. http://www.ferropermoptics.dk

[14] Ocean Optics. USB2000 Data Sheet - Retrieved October 2010. [Online]. http://www.oceanoptics.com/technical/engineering/USB2000%20OEM%20Data%20Sheet.pdf

Appendix -

Ocean Optics USB2000 specifications [14]

USB2000 Specifications

The following sections provide specification information for the CCD Detector in the USB2000, as well as the USB2000 Spectrometer itself.

CCD Detector Specifications

Detector:	Sony ILX511 linear silicon CCD array
Number of elements:	2048 pixels
Pixel size:	14 µm x 200 µm
Pixel well depth:	62,500 electrons
Signal-to-noise ratio:	250:1 (at full signal)
A/D resolution:	12 bit
Dark noise:	2.5 RMS counts
Corrected linearity:	>99.8%

USB2000 Spectrometer Specifications

Dimensions:	89.1 mm x 63.3 mm x 34.4 mm
Weight:	190 g (without cable)
Power consumption:	90 mA @ 5 VDC
Detector range:	200-1100 nm
Detector:	2048-element linear silicon CCD array
Gratings:	14 gratings; UV through Shortwave NIR
Entrance aperture:	5, 10, 25, 50, 100 or 200 mm wide slits or fiber (no slit)
Order-sorting filters:	Installed longpass and bandpass filters
Focal length:	f/4, 42 mm (input); 68 mm (output)
Optical resolution:	~0.3-10.0 nm FWHM (depending on grating and size of entrance aperture)
Dynamic range:	2 x 10^8 (system); 2000:1 for a single scan
Stray light:	<0.05% at 600 nm; <0.10% at 435 nm; <0.10% at 250 nm
Sensitivity (estimate):	400 nm – 90 photons/count; 600 nm – 41 photons/count; 800 nm – 203 photons/count
Fiber optic connector:	SMA 905 to single-strand optical fiber (0.22 NA)
Data transfer rate:	Full scans into memory every 13 milliseconds
Integration time:	3 milliseconds to 65 seconds
Fiber optic connector:	SMA 905 to single-strand optical fiber (0.22 NA)
Operating systems:	Windows 98/Me/2000/XP when using the USB interface on a desktop or notebook PCs Any 32-bit Windows operating system when using the serial port on desktop or notebook PCs Windows CE 2.11 and above when using the serial port on palm-sized PCs

Appendix - Filter specifications

JOHN-V-25 filter

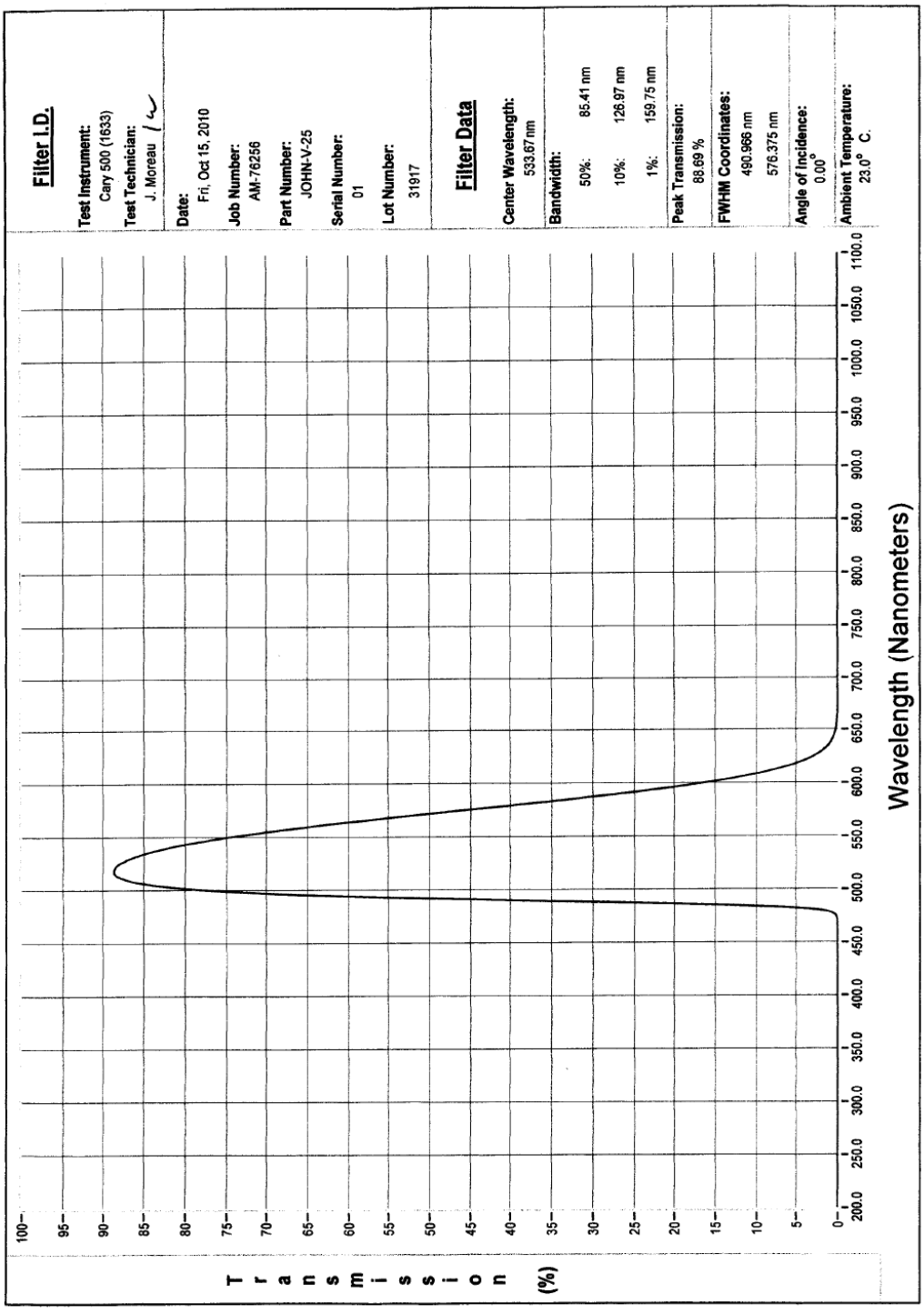

JOHN-B-25 filter

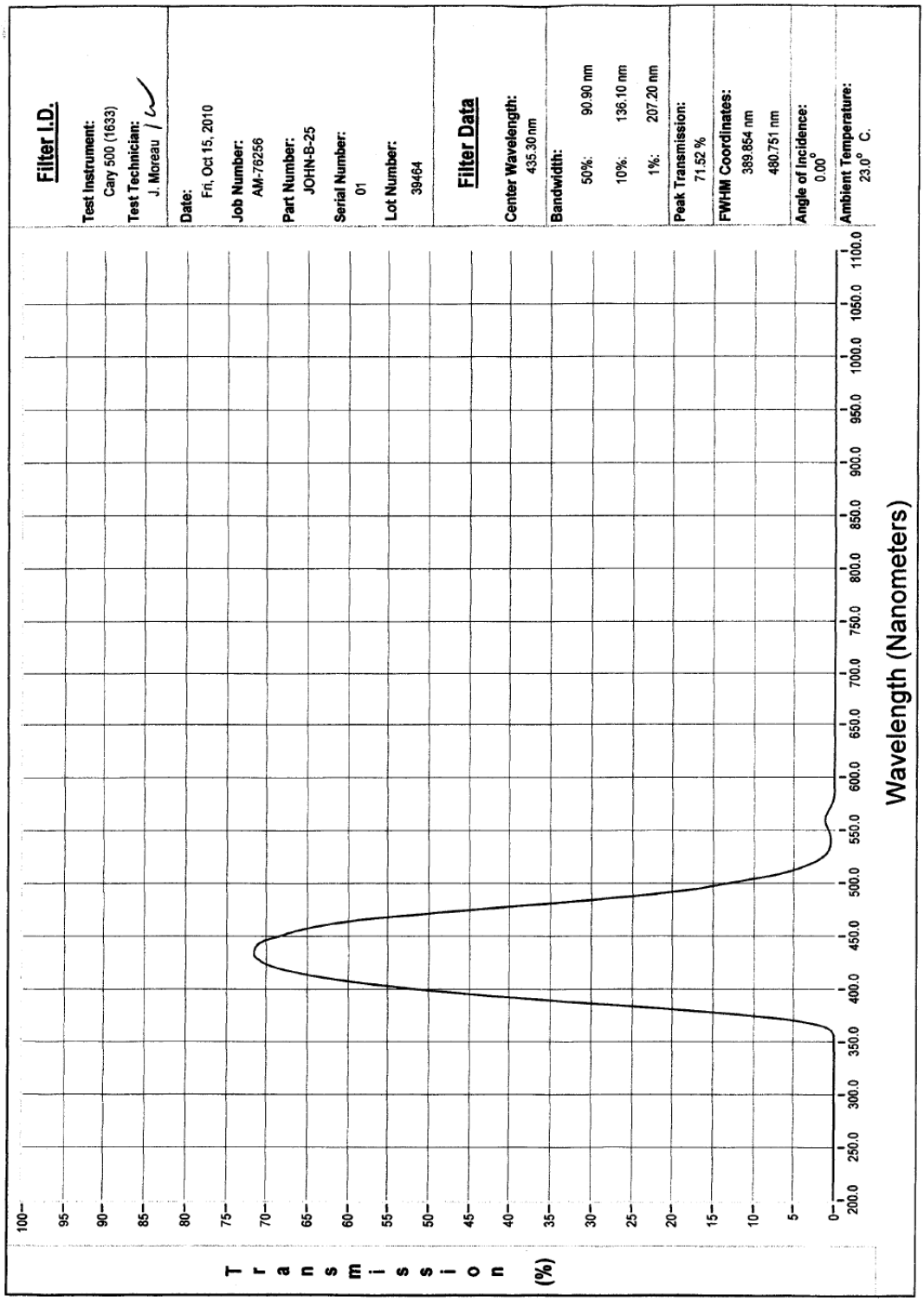

Shortpass filter

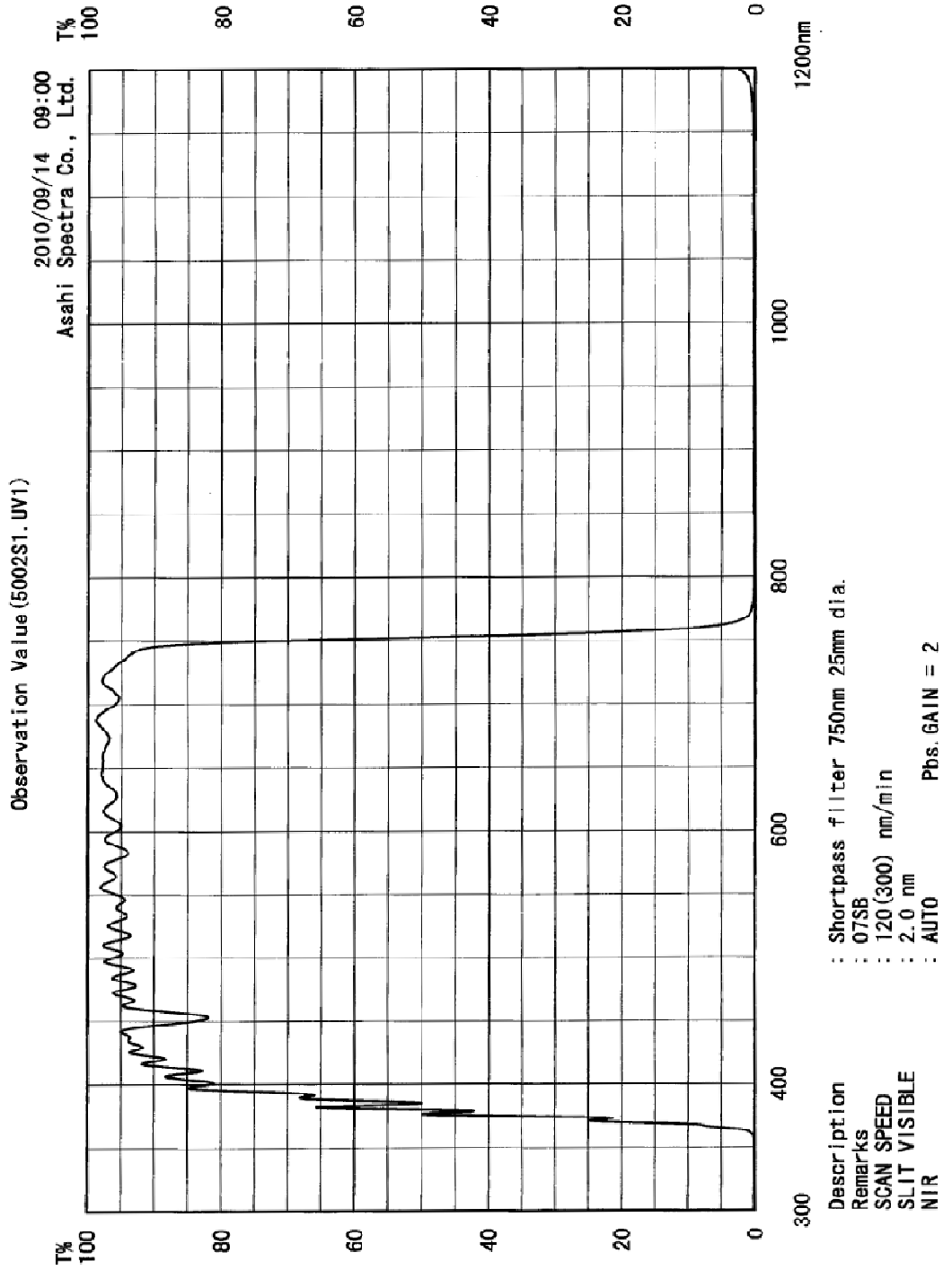

Longpass filter

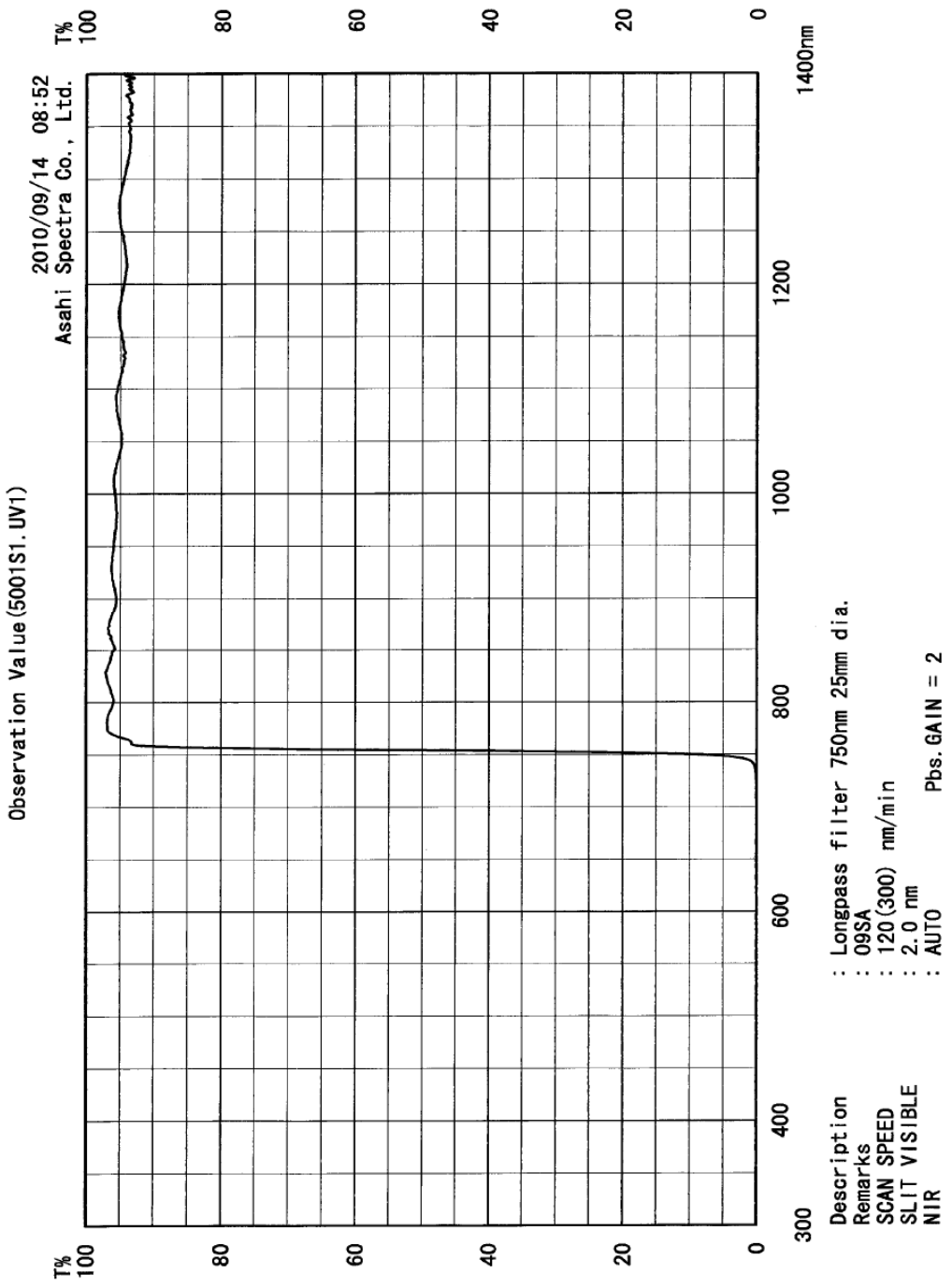

Knife edges specifications

Ferroperm Optics A/S

08-03-2010 14:55:11

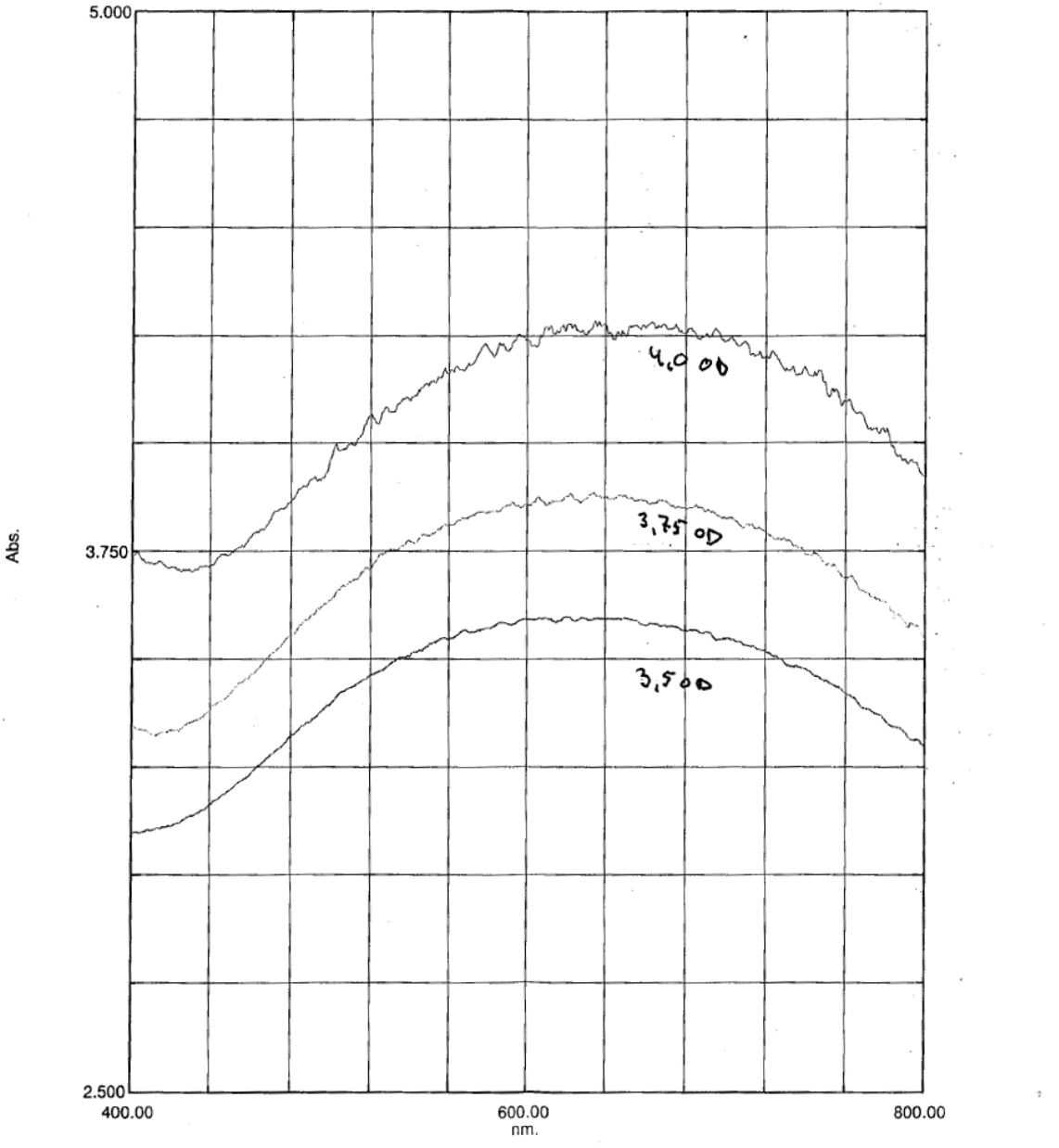

Appendix – Measured spectral transmittance

JOHN-V-25 filter

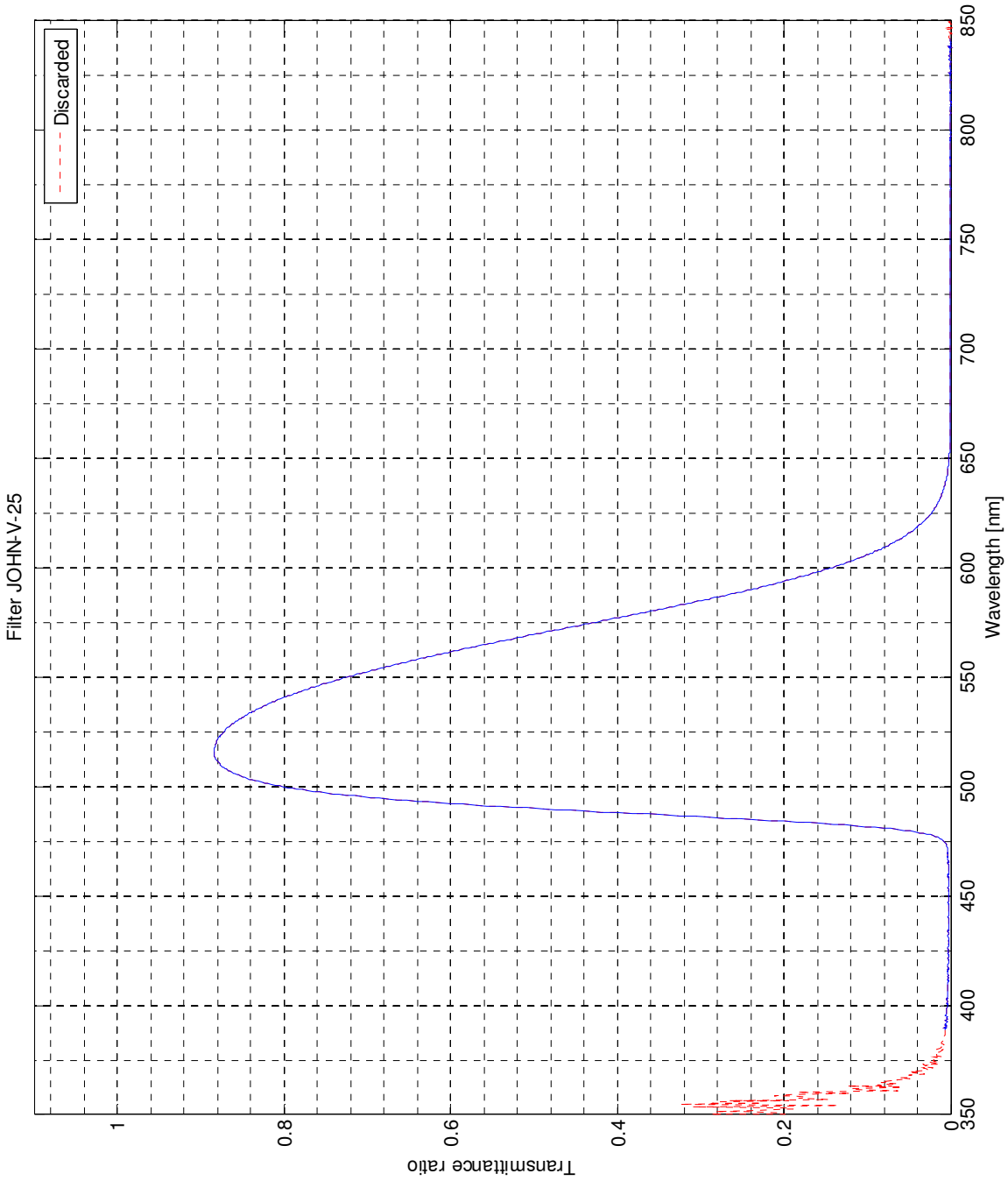

JOHN-B-25 filter

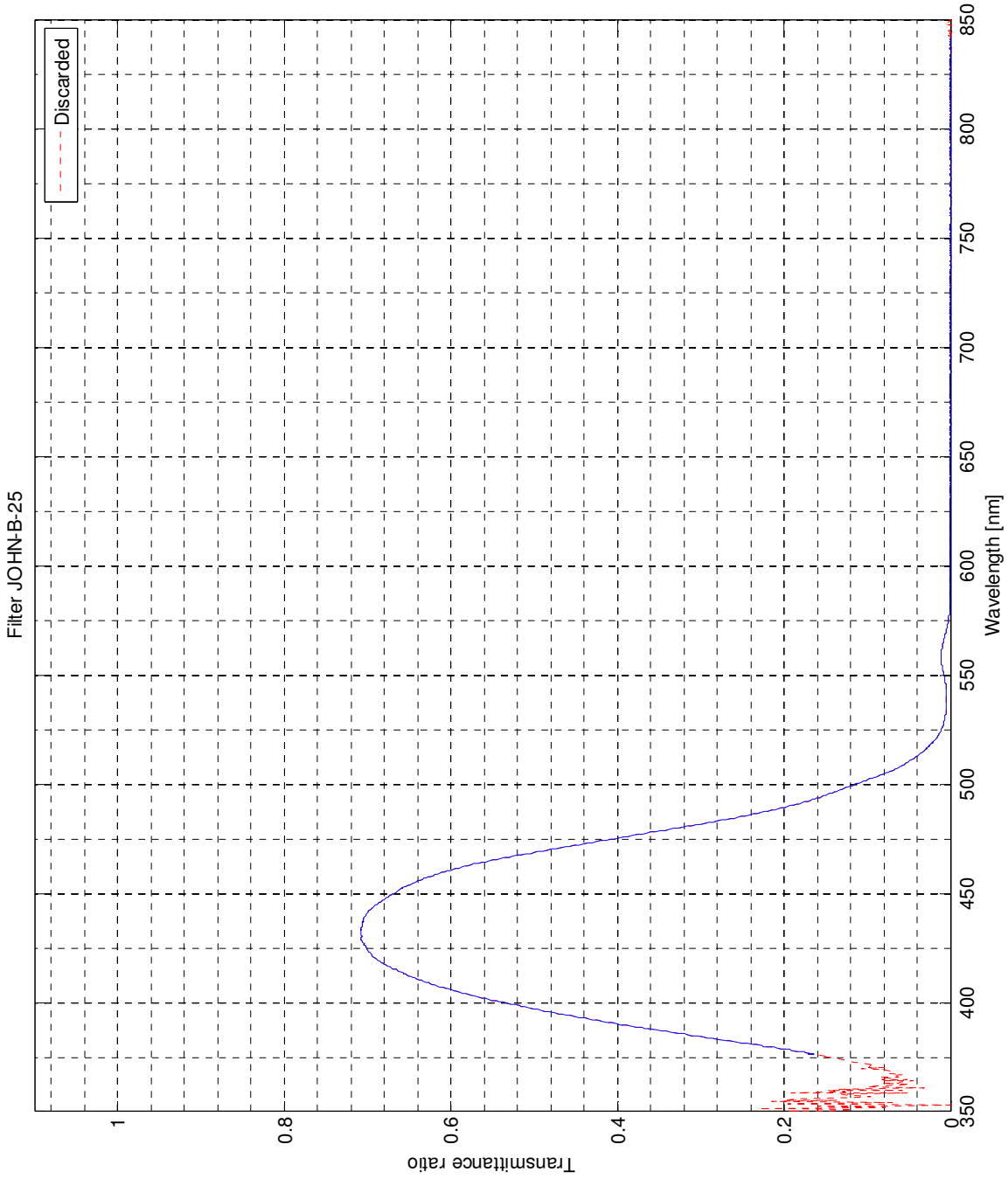

Shortpass filter

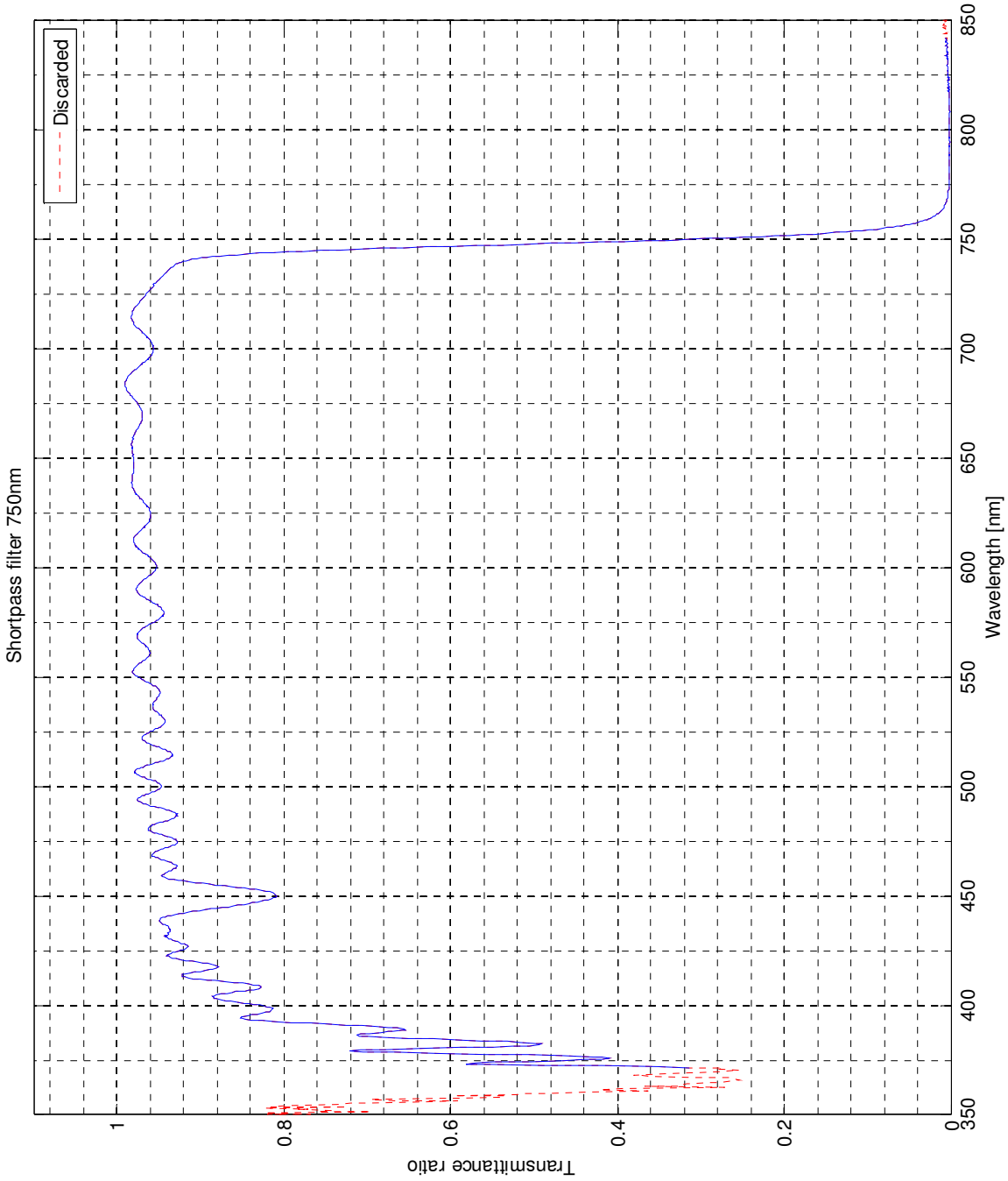

Longpass filter

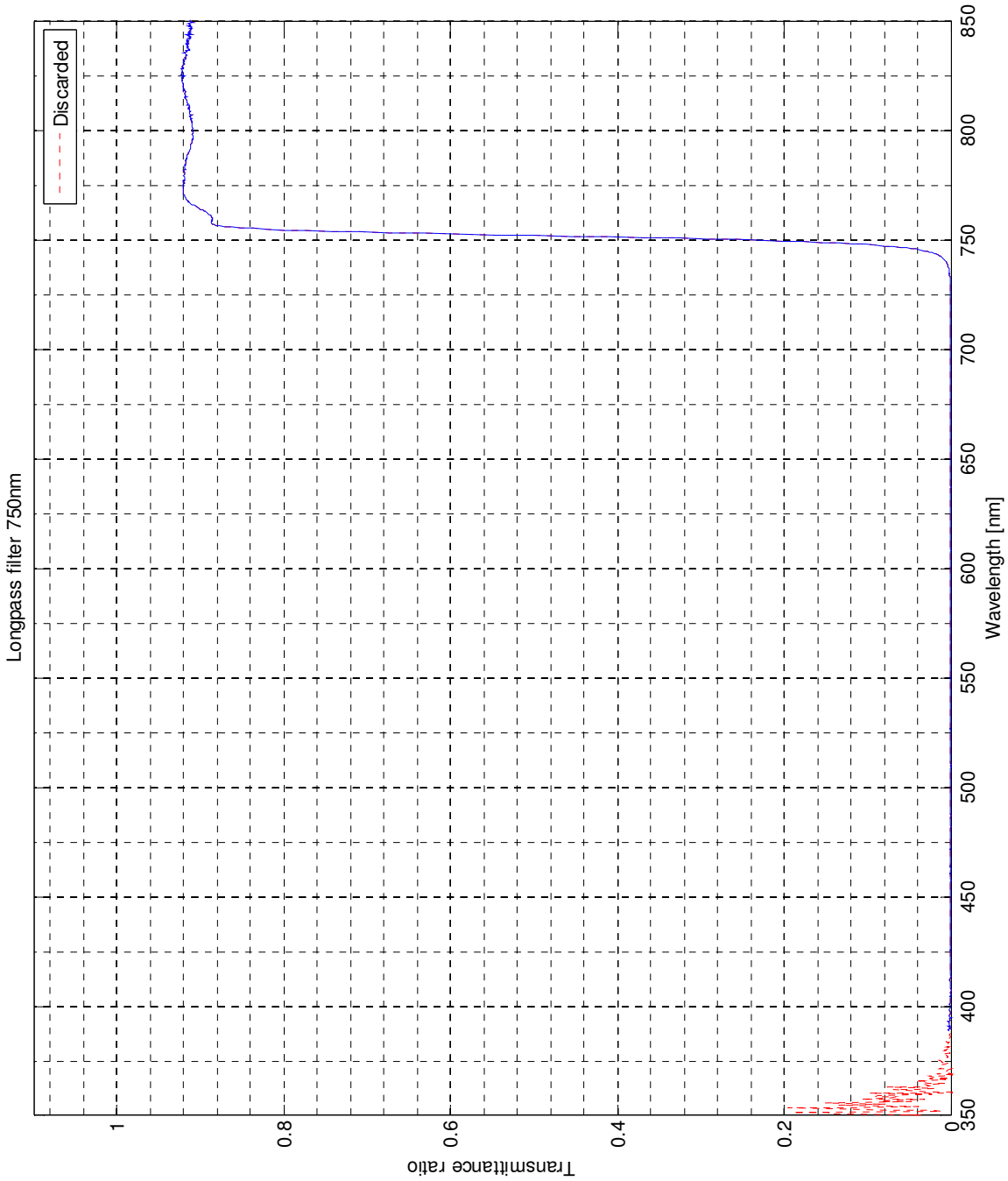

Knife edge OD=3.5

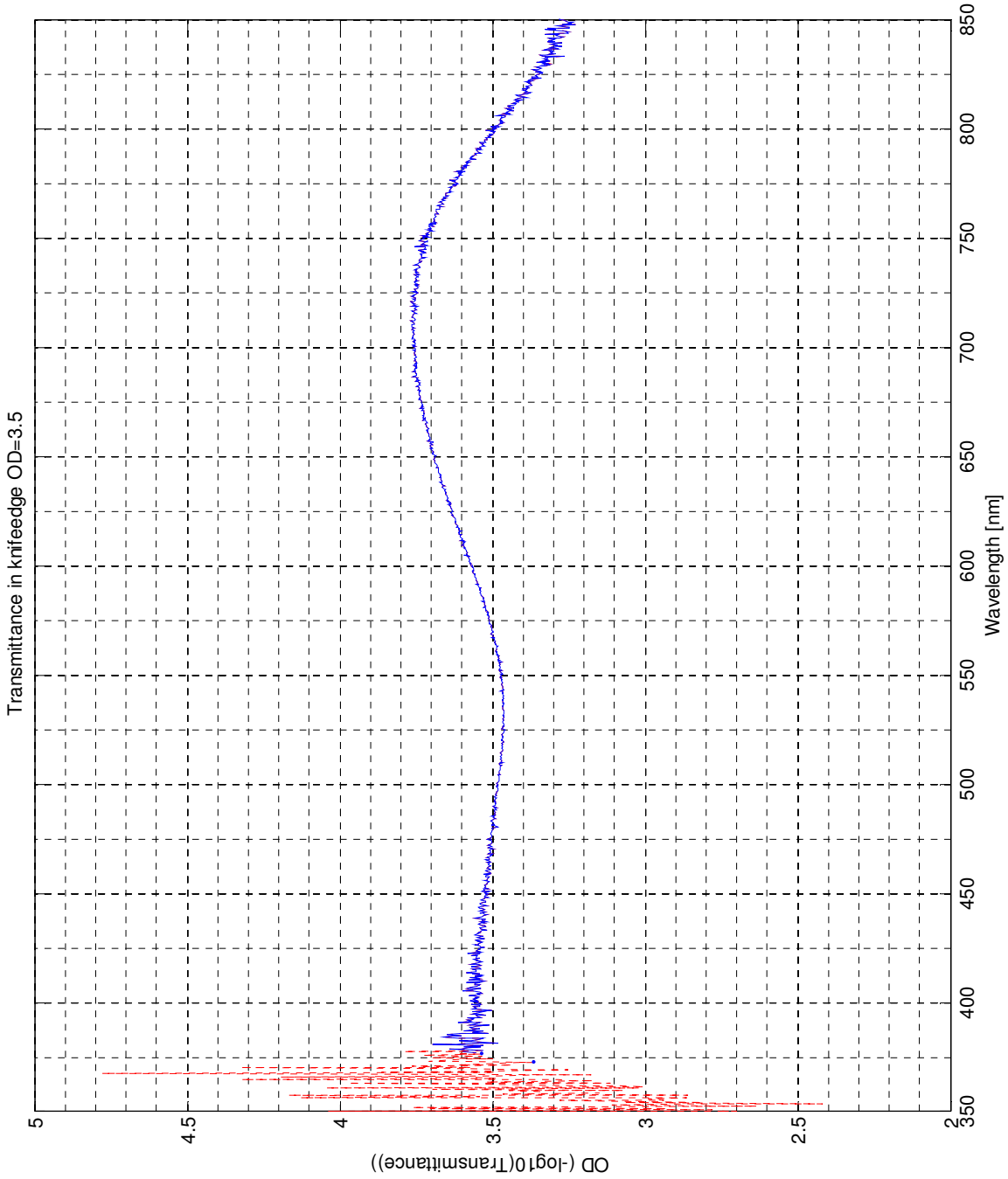

Knife edge OD=3.75

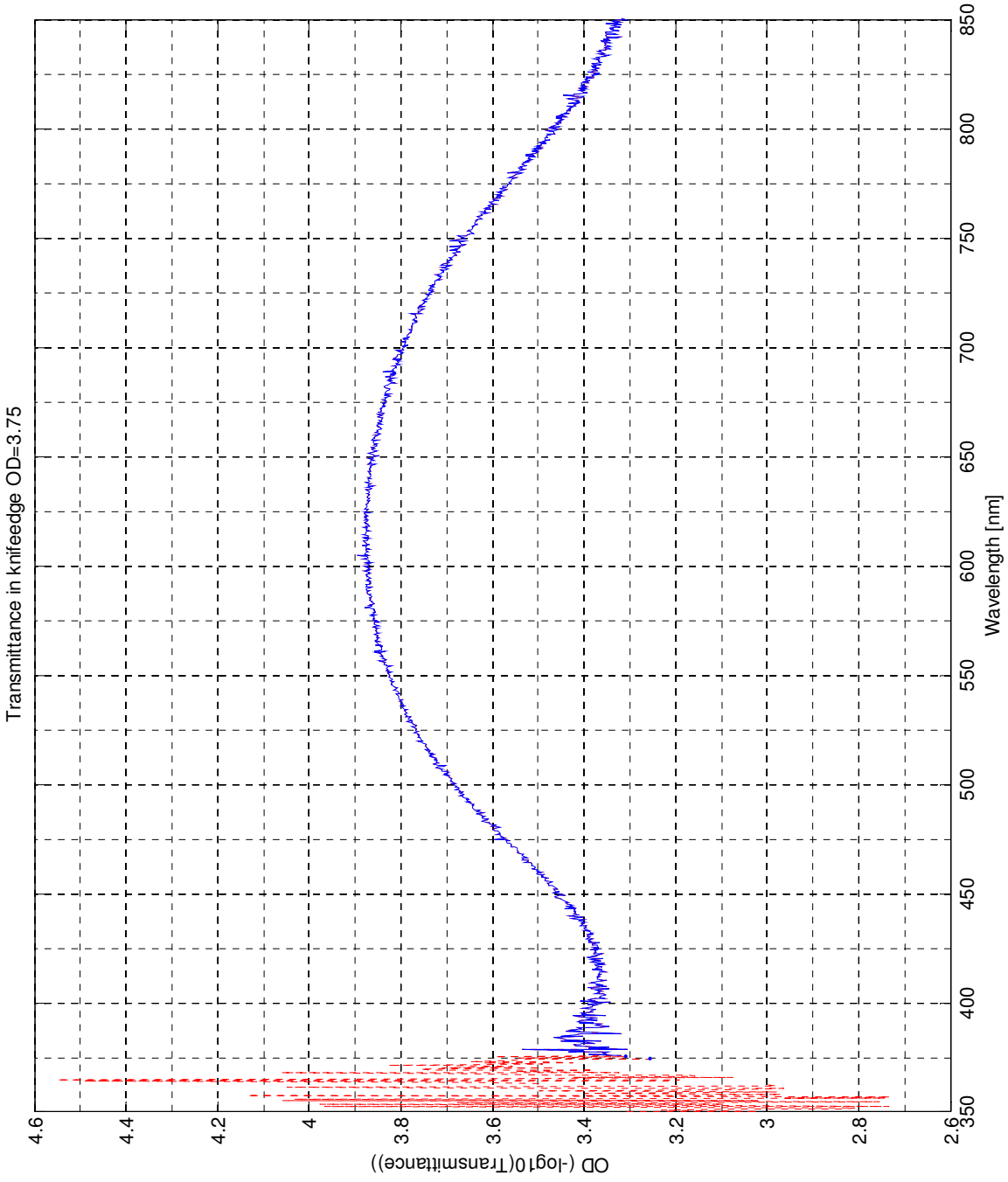

Knife edge OD=4